CANCER

UFMylation maintains tumor suppressor pVHL stability by activating the deubiquitinase BAP1

Xiao Yang[1]†, Yalei Wen[2]†, Shengying Qin[3,4]†, Yang Zhou[1]†, Caishi Zhang[1], Lei Huang[1], Mei Li[1], Xiuqing Ma[1], Rui Wan[1], Jiaqi Chen[1], Rong-Rong He[1,5,6], Hao Gao[6], Colin R. Goding[7], Oscar Junhong Luo[8]*, Xiangchun Shen[9]*, Rutao Cui[10]*, Tongzheng Liu[1,9]*

***BRCA1-associated protein 1* (*BAP1*) can function as a tumor suppressor or oncogene depending on context, but its role in colorectal cancer (CRC) is not well understood. Here, we demonstrate that BAP1 suppresses CRC progression primarily by deubiquitinating and stabilizing von Hippel–Lindau tumor suppressor protein (pVHL). BAP1 undergoes covalent modification by ubiquitin-fold modifier 1 (UFM1) at Lys[51], Lys[61], Lys[187], and Lys[205], enhancing its interaction with pVHL and promoting pVHL stabilization. Loss of this modification through UFL1 depletion or reconstitution with a UFMylation-defective BAP1 mutant (4KR) impairs pVHL stabilization and promotes tumor progression in CRC cell line–based and patient-derived xenograft models. Clinically, down-regulation of UFL1 and BAP1 correlates with reduced pVHL level and poor prognosis in patients with CRC. These findings identify a previously unrecognized posttranslational mechanism regulating BAP1 activity and highlight UFMylation as essential for maintaining pVHL tumor-suppressive function. Targeting BAP1 UFMylation may represent a potential therapeutic strategy in CRC and other cancers with wild-type *BAP1* and *VHL*.**

INTRODUCTION

Colorectal cancer (CRC) is one of the most prevalent cancers and a leading cause of cancer-related death worldwide (*1*). Despite advancements in early diagnosis and systemic therapies for CRC, the prognosis for advanced CRC remains poor, with a dismal 5-year survival rate due to metastasis and resistance to existing therapies (*2*). Thus, to elucidate the key mechanisms driving CRC progression and to identify potential therapeutic targets are urgently needed.

Recent evidence suggests that the role of BRCA1-associated protein 1 (BAP1) in cancer is highly context dependent, varying across cell types. Frequent mutations or deletions in the *BAP1* gene are associated with a high incidence of malignant mesothelioma, clear cell renal cell carcinoma (ccRCC), and uveal melanoma (*3*–*5*). In murine models, heterozygous loss of BAP1 in the pancreas causes pancreatitis and, in combination with $Kras^{G12D}$ expression, leads to rapid progression to metastatic pancreatic cancer, suggesting that BAP1 acts as a haploinsufficient tumor suppressor in pancreatic cancer (*6*). Furthermore, BAP1 exerts tumor-suppressive effects in intrahepatic cholangiocarcinoma and clear cell renal carcinoma by inhibiting extracellular signal–regulated kinase 1/2–c-Jun N-terminal kinase/c-Jun pathway or regulating SLC7A11 expression through the deubiquitination of histone 2A (H2A) to induce ferroptosis (*7*, *8*). In contrast, BAP1 can also exhibit oncogenic activity. Truncation mutations of Additional Sex Combs Like 1 (ASXL1), a BAP1-associated protein, have been showed to increase BAP1 protein stability, driving a pro-leukemic transcriptional signature and promoting leukemogenesis (*9*, *10*). Additionally, ASXL3 functions as an adaptor protein linking BRD4 to the BAP1 complex, regulating enhancer activity and promoting small cell lung cancer (SCLC). Inhibition of BAP1 in SCLC disrupts the BAP1/ASXL3/BRD4 epigenetic axis, inducing protein ASXL3 degradation and suppressing tumor growth in vivo (*11*, *12*). Furthermore, BAP1 has been implicated in promoting breast cancer proliferation and metastasis by deubiquitinating KLF5 (*13*). However, despite these notable findings, the role of BAP1 in CRC remains poorly understood.

Our analysis of the cBioPortal database revealed that the *BAP1* gene in CRC is largely wild type (WT), and its expression is down-regulated in primary CRC specimens and even more significantly in metastatic CRC specimens. Additionally, we demonstrated that BAP1 plays a tumor-suppressive role in CRC primarily by deubiquitinating and stabilizing the key tumor suppressor protein pVHL, without affecting other known BAP1 substrates such as LKB1 and SLC7A11, which are implicated in other cancers (*7*, *14*).

The regulation of BAP1 in human cancers is also not well understood. BAP1 has been reported to undergo several posttranslational modifications, including phosphorylation and ubiquitination, which influence its subcellular localization (*15*–*18*). However, the mechanisms regulating BAP1's activity toward its substrates in cancer contexts remain largely unclear. In this study, we demonstrate that BAP1 can be covalently modified by ubiquitin-fold modifier 1 (UFM1), a recently identified ubiquitin-like modification (*19*–*23*). Notably, the UFMylation at specific lysine residues (Lys[51], Lys[61], Lys[187], and Lys[205]) in BAP1 substantially enhances its specific interaction with pVHL,

[1]State Key Laboratory of Bioactive Molecules and Druggability Assessment/International Cooperative Laboratory of Traditional Chinese Medicine Modernization and Innovative Drug Development of Ministry of Education (MOE) of China/College of Pharmacy, Jinan University, Guangzhou 510632, China. [2]Guangdong Second Provincial General Hospital, Postdoctoral Station of Traditional Chinese Medicine, School of Medicine, Jinan University, Guangzhou 510632, China. [3]Department of Oncology, The First Affiliated Hospital of Jinan University, Guangzhou 510630, China. [4]Clinical Medical Research Institute, Jinan University, Guangzhou 510630, China. [5]Guangdong Engineering Research Center of Chinese Medicine and Disease Susceptibility, Jinan University, Guangzhou 510632 China. [6]Institute of Traditional Chinese Medicine and Natural Products, College of Pharmacy/State Key Laboratory of Bioactive Molecules and Druggability Assessment/International Cooperative Laboratory of Traditional Chinese Medicine Modernization and Innovative Drug Development of Ministry of Education (MOE) of China/Guangdong Province Key Laboratory of Pharmacodynamic Constituents of TCM and New Drugs Research, Jinan University, Guangzhou 510632, China. [7]Ludwig Institute for Cancer Research, Nuffield Department of Clinical Medicine, University of Oxford, Headington, Oxford OX3 7DQ, UK. [8]Department of Systems Biomedical Sciences, School of Medicine, Jinan University, Guangzhou 510632, China. [9]The State Key Laboratory of Functions and Applications of Medicinal Plants, Guizhou Medical University, Guiyang 550014, China. [10]Zhejiang University School of Medicine, Hangzhou 310058, China.
*Corresponding author. Email: liutongzheng@jnu.edu.cn (T.L.); rutaocui@zju.edu.cn (R.C.); sxc@gmc.edu.cn (X.S.); luojh@jnu.edu.cn (O.J.L.)
†These authors contributed equally to this work.

promoting the deubiquitination and stabilization of pVHL in CRC. Conversely, loss of UFMylation, either through UFL1 depletion or reconstitution with the UFMylation-defective BAP1 mutant 4KR, fails to stabilize pVHL efficiently, thereby promoting CRC progression both in vitro and in vivo. Clinically, down-regulation of UFL1 and BAP1 in CRC specimens correlates with reduced pVHL levels and poor prognosis in patients with CRC. In summary, our findings identify UFMylation as a critical posttranslational mechanism regulating BAP1 activity and its role in maintaining pVHL stability and tumor-suppressive function. These results suggest that targeting BAP1 UFMylation could be a promising therapeutic strategy for CRC and potentially other cancers with WT *BAP1* and *VHL*.

RESULTS

BAP1 exerts a tumor-suppressive role in CRC

Alterations in the *BAP1* gene are frequently detected in several human cancers, including malignant mesothelioma (*3*) and melanoma (*5*). However, the status and role of BAP1 in CRC has not been well characterized. To address this, we analyzed *BAP1* alterations in CRC using cBioPortal for Cancer Genomics databases and found that the *BAP1* gene is predominantly WT in CRC (fig. S1A). To further investigate BAP1 expression, we reanalyzed two independent single-cell RNA sequencing (scRNA-seq) datasets of human CRC (Gene Expression Omnibus: GSE132257 and GSE132465), which include data from 23 and 5 primary CRC samples and their matched normal mucosa, respectively (*24*). Both datasets demonstrated significantly lower *BAP1* expression in the epithelial cells of CRC tumors compared to normal mucosa tissues (Fig. 1A). Consistent with these findings, analysis from The Cancer Genome Atlas (TCGA) datasets also revealed a notable down-regulation of *BAP1* expression in CRC relative to normal tissues (fig. S1B). To validate these observation at the protein level, we performed immunoblotting and immunohistochemistry (IHC) analyses. These experiments confirmed reduced BAP1 protein expression in primary CRC specimens compared to that in adjacent normal tissues (Fig. 1, B and C). Notably, BAP1 expression was even more significantly reduced in metastatic tissues than adjacent normal tissues (Fig. 1C). Additionally, Kaplan-Meier plot analysis indicated that higher BAP1 expression in CRC correlates with improved recurrence-free survival (fig. S1C).

To investigate the functional role of BAP1 in CRC, we overexpressed WT BAP1 (WT) in CRC cells. This overexpression led to a marked reduction in cell proliferation, migration, and invasion, as well as increased sensitivities to cisplatin and 5-fluorouracil (5-FU). In contrast, overexpression of a catalytically inactive mutant (BAP1 C91S) did not elicit these effects (Fig. 1, D and E, and fig. S1D). Consistent with this, a similar effect was observed in CRC cell–based xenograft experiments (Fig. 1F). Conversely, the knockdown of BAP1 enhanced cell proliferation, migration, and invasion of CRC cells, as well as reduced chemosensitivity (Fig. 1, G and H; and fig. S1, E and F). The tumor-suppressive role of BAP1 was further supported by in vivo xenograft experiments (Fig. 1I). In tumors from mice treated with saline or cisplatin, BAP1 depletion in HCT116 cells led to a marked increase in Ki67 expression and a reduction in apoptosis, as indicated by decreased cleaved caspase-3 staining (fig. S1G). Collectively, our findings suggest that BAP1 functions as a tumor suppressor in CRC, with its down-regulation correlating with poor clinical outcomes. These results underscore the potential of BAP1 as a therapeutic target in CRC.

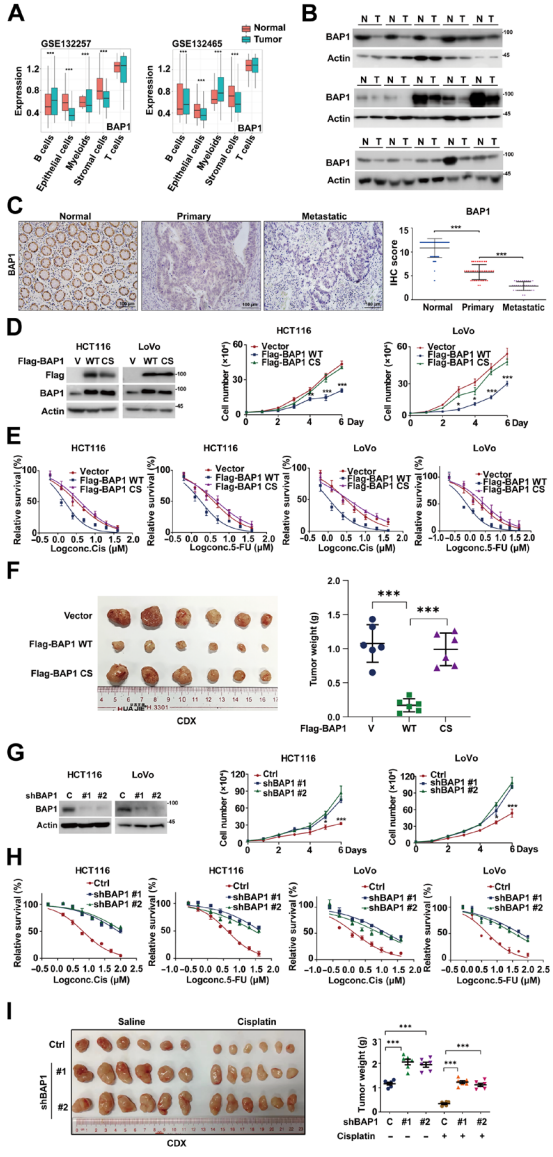

Fig. 1. BAP1 exerts a tumor-suppressive role in CRC. (**A**) Reanalysis of BAP1 expression across five cell types in patients with CRC using scRNA-seq datasets (GSE132257 and GSE132465), comparing tumor and matched normal mucosa ($n = 5$), and in a larger cohort of CRC tumor ($n = 23$) and matched normal mucosa samples ($n = 10$). (**B**) BAP1 expressions were assessed in CRC and adjacent normal tissues (N, normal; T, tumor). (**C**) Representative immunohistochemical staining of BAP1 in normal ($n = 73$), primary ($n = 38$), and metastatic ($n = 35$) CRC tissues, with corresponding IHC score analysis. (**D**) HCT116 and LoVo cells stably expressing vector, Flag-BAP1 WT, or Flag-BAP1 C91S (CS) mutant were generated, and Western blotting was performed. Cell proliferation assay was performed. Data are shown as means ± SD ($n = 3$). (**E**) Cells in (D) were treated with cisplatin or 5-FU. Cell survival was determined. Data are shown as means ± SD ($n = 4$). (**F**) HCT116 cells (1×10^6) in (D) were subcutaneously implanted into nude mice ($n = 6$). Tumors were harvested at endpoint and weighed (means ± SD). (**G**) HCT116 and LoVo cells stably expressing control or BAP1 shRNAs were analyzed by Western blotting and subjected to proliferation assay. Data are shown as means ± SD ($n = 3$). (**H**) Cells in (G) were treated with cisplatin (Cis) or 5-FU. Cell survival was determined. Data are shown as means ± SD ($n = 4$) (**I**) HCT116 cells (1×10^6) in (G) were subcutaneously implanted into nude mice. Upon reaching about 100 mm^3, mice were treated with saline or cisplatin (2 mg/kg weekly, $n = 6$). Tumors were weighed at endpoint and analyzed. Data are shown as means ± SD and were analyzed using one-way analysis of variance (ANOVA). *$P < 0.05$; ***$P < 0.001$.

BAP1 deubiquitinates and stabilizes pVHL

Accumulating evidence suggests that BAP1 exerts its effects on substrates in a context-dependent manner, either suppressing or promoting tumor progression (*7*, *13*, *25*). To investigate it in the context of CRC, we first examined the expression levels of Phosphatase and Tensin Homolog (PTEN), Liver Kinase B1 (LKB1), and Solute Carrier Family 7 Member 11 (SLC7A11), previously reported substrates of BAP1 in prostate cancer, lung cancer, and kidney clear cell carcinoma, respectively (*7*, *14*, *26*). As shown in fig. S2A, BAP1 depletion in CRC cells did not significantly affect the protein levels of PTEN, LKB1, and SLC7A11. To identify CRC-specific substrates of BAP1, we performed tandem affinity purification and mass spectrometry (MS) analysis using HCT116 cells stably expressing Flag-S-BAP1. In addition to some known BAP1 interacting proteins such as FOXK1 (*27*, *28*) and HCFC1 (*27*, *29*), we identified the von Hippel–Lindau protein pVHL as a previously unrecognized interactor of BAP1 in CRC cells (Fig. 2A). The endogenous interaction between BAP1 and pVHL was further validated through co-immunoprecipitation assays in HCT116 cells (Fig. 2B). Additionally, in vitro binding assays demonstrated that purified glutathione *S*-transferase (GST)–BAP1, but not GST alone, could directly interact with recombinant His-VHL, confirming a direct interaction between BAP1 and pVHL (Fig. 2C). To further map this interaction, we generated several BAP1 fragment constructs on the basis of the functional domains and found that both full-length BAP1 (FL) and its N-terminal region (amino acids 1 to 240) could directly interact with pVHL (Fig. 2D).

pVHL is a key tumor suppressor that targets hydroxylated hypoxia-inducible factor α (HIFα), Akt, and other substrates for degradation or inactivation. pVHL is frequently down-regulated in cancers harboring WT *VHL* (*30*, *31*). As shown in fig. S2B, the *VHL* gene is predominantly WT in CRC, with a mutation frequency of less than 1%. This contrasts with its frequent mutations or loss in ccRCC (*30*). Given the direct interaction between BAP1 and pVHL, thus, we further investigated whether BAP1 could suppress CRC progression by regulating pVHL stability and function. As shown in Fig. 2E and fig. S2C, BAP1 depletion in CRC cells resulted in a marked decrease in pVHL protein levels, accompanied by the accumulation of HIF-1α and increased expressions of HIF-1α target genes *VEGF* and *MMP2*. We reanalyzed publicly available scRNA-seq data (GEO: GSE132465), which include samples from 23 patients with primary CRC and 10 matched normal mucosae. As shown in Fig. 2F, canonical HIF-1 target genes, including *CCND1*, *MYC*, *SLC2A1*, *LDHA*, *BNIP3*, *CDK4*, *MET*, and *BHLHE40*, were significantly up-regulated in epithelial cells of CRC tumors compared to those of matched normal tissues. Consistent with these findings, RNA sequencing (RNA-seq) of BAP1-depleted HCT116 cells revealed a significant enrichment of HIF-1 signaling-associated genes (Fig. 2, G and H), including up-regulation of HIF-1α target genes (e.g., *MYC*, *SLC2A1*, and *LDHA*) and down-regulation of HIF-1α–repressed genes, including *CAD* and *CDH1* (*32*–*34*). This transcriptional profile supports the mechanistic link between BAP1 loss, pVHL destabilization, and enhanced HIF-1α signaling in CRC cells. Conversely, the overexpression of BAP1 WT, but not the catalytically inactive C91S mutant, markedly increased pVHL protein levels (fig. S2D). Notably, this regulation occurred at the post-translational level, as no significant differences in *VHL* mRNA levels were observed upon BAP1 depletion or overexpression in CRC cells (fig. S2E). Further investigation revealed that treatment with the proteasome inhibitor MG132 rescued the reduced pVHL protein levels in BAP1-deficient HCT116 cells, suggesting that BAP1 stabilizes pVHL by preventing its proteasomal degradation (Fig. 2I). Additionally, cycloheximide pulse-chase assay demonstrated that BAP1 depletion significantly reduced the half-life of pVHL, whereas overexpression of BAP1 WT, but not the C91S mutant, markedly stabilized pVHL protein in HCT116 cells (Fig. 2J and fig. S2F).

Given that the direct deubiquitinase (DUB) for pVHL has not yet been identified, we sought to determine whether BAP1 acts as the bona fide DUB for pVHL. Our data demonstrate that depletion of BAP1 markedly increased the ubiquitination level of pVHL (Fig. 2K). Furthermore, cells transfected with BAP1 WT, but not the C91S mutant, exhibited a notable decrease in polyubiquitylated pVHL (fig. S2G). Additionally, incubation with purified GST-BAP1 WT in vitro, but not the C91S mutant, caused a notable reduction in polyubiquitinated pVHL (fig. S2H). We also found that BAP1 WT rather than the C91S mutant catalyzed the cleavage of K48, but not K63-specific polyubiquitin chain (fig. S2I). While OTUD6B has been reported to regulate pVHL stability by modulating the interaction between pVHL and the ubiquitin E3 ligase WD repeat and SOCS box-containing protein 1 (WSB1) in an enzyme-independent manner in hepatocellular carcinoma (*35*, *36*), our results showed that the BAP1 depletion had minimal impact on the pVHL-WSB1 interaction in HCT116 cells (fig. S2J), suggesting that BAP1 serves as the DUB for pVHL in CRC.

BAP1 suppresses tumor progression through stabilizing pVHL

pVHL has been well-documented as a tumor suppressor in melanoma and other cancers harboring WT *VHL* (*35*). We further validated the tumor-suppressive role of pVHL in CRC, as pVHL depletion led to a marked increase of cell growth, migration, and invasion, while overexpression of pVHL strongly suppresses these phenotypes (fig. S3, A to D). Given the role of BAP1 in deubiquitinating and stabilizing pVHL, we next investigated whether the tumor-suppressive effects of BAP1 in CRC are mediated through pVHL. As shown in Fig. 3 (A and B) and fig. S3 (E and F), reconstitution of Flag-VHL significantly inhibited the increased cell proliferation and enhanced cellular sensitivity to cisplatin and 5-FU in BAP1-depleted cells. This effect was also observed in CRC cell–based xenograft experiments and patient-derived xenograft (PDX) models (Fig. 3, C and D). In addition, we examined the potential functions of the BAP1-pVHL axis in other tumor types. As shown in fig. S3 (G and H), BAP1 depletion in pancreatic cancer (AsPC-1 and MIA PaCa-2 cells) and ovarian cancer (A2780 and SKOV3 cells) also resulted in a significant decrease in pVHL protein levels and enhanced cell proliferation as well as reduced chemosensitivity. The reconstitution of Flag-VHL significantly inhibited the increased cell proliferation and enhanced cellular chemosensitivity in BAP1-depleted cells. Furthermore, we explored whether BAP1 regulates CRC metastasis in a pVHL-dependent manner, as metastasis remains the primary cause of CRC-related mortality (*2*). As shown in Fig. 3E and fig. S3I, BAP1 depletion in CRC cells significantly promoted migration, invasion, and liver metastasis, which was markedly reversed by reconstitution of Flag-VHL in BAP1-depleted cells. These findings underscore that the tumor-suppressive activity of BAP1 in CRC is predominantly mediated through the stabilization of pVHL.

UFL1 interacts with and UFMylates BAP1 at Lys^{51}, Lys^{61}, Lys^{187}, and Lys^{205}

While various substrates of BAP1 have been identified in previous study, the mechanisms regulating BAP1 activity toward substrates

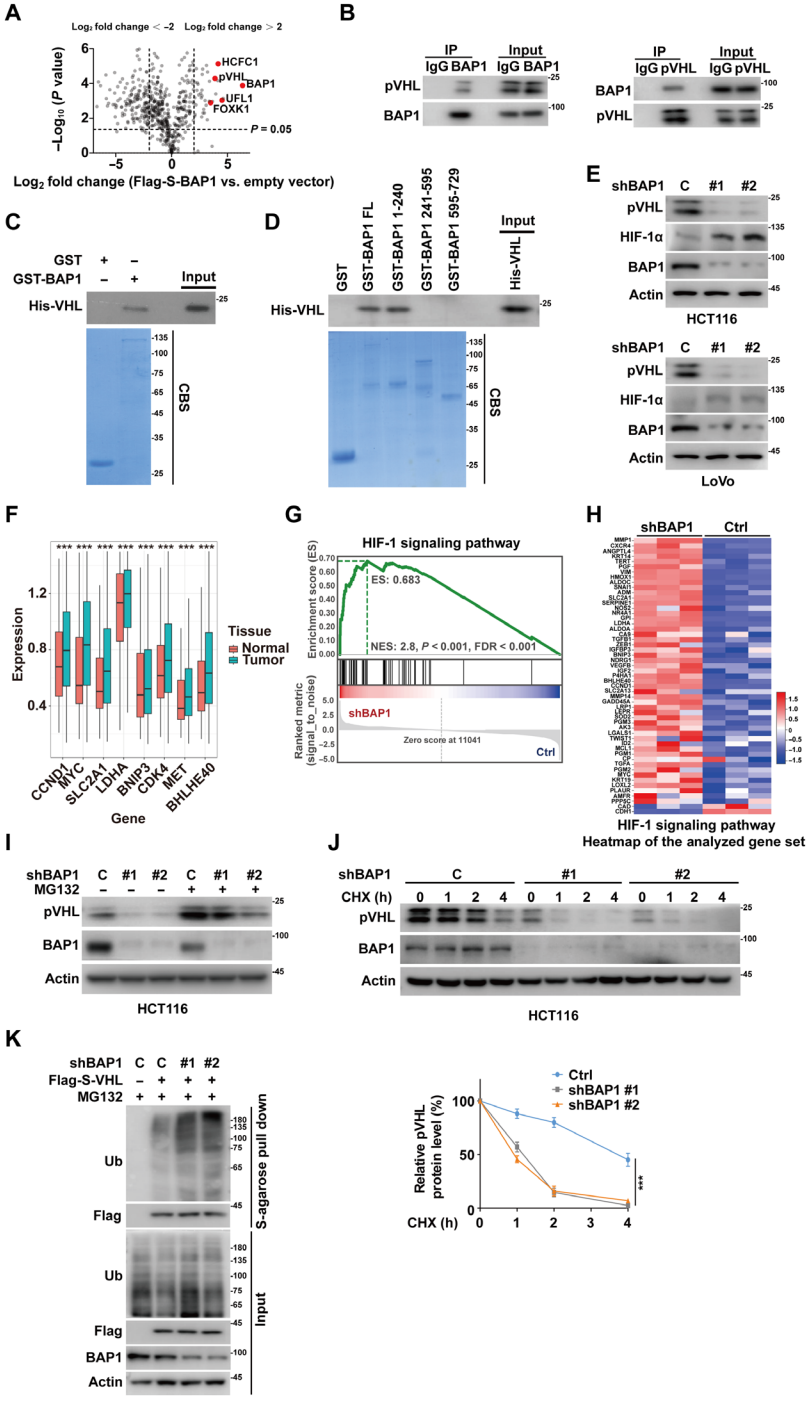

Fig. 2. BAP1 deubiquitinates and stabilizes pVHL. (**A**) Volcano plot of BAP1-associated proteins identified by MS in HCT116 cells stably expressing Flag-S-BAP1 and treated with MG132 (10 μM) for 10 hours. (**B**) Co-immunoprecipitates (Co-IP) in HCT116 cells using immunoglobulin G (IgG), anti-BAP1, or anti-pVHL antibodies followed by immunoblotting with the indicated antibodies. (**C**) In vitro binding assay showing interaction between purified His-VHL and recombinant GST or GST-BAP1. CBS, Coomassie blue staining. (**D**) Mapping of BAP1 regions required for pVHL interaction using GST-fused full-length (FL) and truncated BAP1 proteins incubated with purified His-VHL in vitro. (**E**) Western blotting of HCT116 and LoVo cells stably expressing control or BAP1 shRNAs using the indicated antibodies. (**F**) Reanalysis of scRNA-seq data (GEO: GSE132465) from patients with CRC containing 23 primary CRC tumors and 10 matched normal mucosae. ***$P < 0.001$, Wilcoxon rank sum test, one-sided. (**G**) Gene set enrichment analysis (GSEA) of RNA-seq data from BAP1-depleted HCT116 cells showing significant enrichment of HIF-1 signaling pathway genes. NES, Normalized Enrichment Score. (**H**) Heatmap of HIF-1 target gene expression in BAP1-depleted versus control HCT116 cells by RNA-seq. (**I**) Western blotting of HCT116 cells stably expressing control or BAP1 shRNAs treated with vehicle or MG132 (10 μM) for 10 hours. (**J**) Cycloheximide pulse-chase assay to assess pVHL protein stability in cells as in (E). Data are shown as means ± SD ($n = 3$). h, hours. (**K**) Cells stably expressing control or BAP1 shRNAs were transfected with vector or pIRES-VHL (containing Flag and S tag), then treated MG132 for 10 hours. Cell lysates were pulled down by S-agarose, and the polyubiquitylated pVHL was measured by Western blotting with an anti-ubiquitin antibody. Data are shown as means ± SD and were analyzed by one-way ANOVA. ***$P < 0.001$.

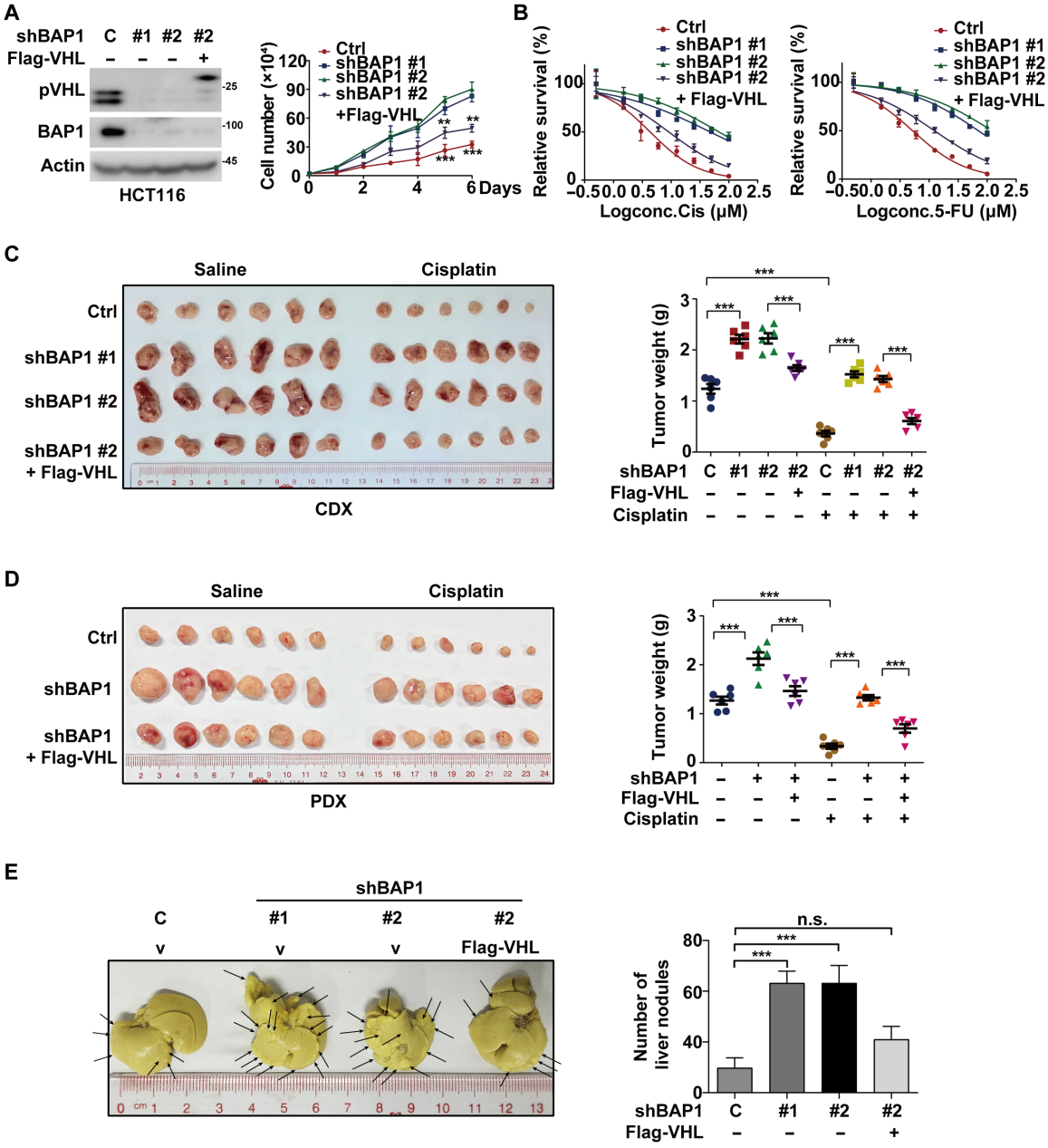

Fig. 3. BAP1 suppresses tumor progression through stabilizing pVHL. (**A**) HCT116 cells stably expressing control or BAP1 shRNAs were transfected with vector or Flag-VHL. The protein levels of BAP1 and pVHL were determined by Western blotting, and cell proliferation was measured. Results represent the means ± SD of three independent experiments. (**B**) Cells as in (A) were treated with the indicated concentrations of cisplatin or 5-FU, and cell survival was determined. Results represent the means ± SD of four independent experiments. (**C**) HCT116 cells expressing control or BAP1 shRNAs and stably reconstituting vector or Flag-VHL were injected subcutaneously in nude mice. When tumor volume reached 100 mm^3, mice were treated with saline or cisplatin (2 mg/kg once a week), respectively ($n = 6$ per group). Tumors were collected at 6 weeks, and tumor weights were measured and analyzed. (**D**) CRC patient-derived xenografts (PDXs) were subcutaneously implanted into nude mice. Xenograft tumors were injected with lentivirus expressing the indicated constructs when tumor volume reached 30 mm^3. Mice were then treated with saline or cisplatin (2 mg/kg once a week), respectively ($n = 6$ per group). Tumors were collected, and tumor weights were measured and analyzed. Results represent the means ± SD from six mice. (**E**) HCT116 cells expressing control or BAP1 shRNAs were stably reconstituted with vector or Flag-VHL and injected into the spleen of nude mice ($n = 6$ per group). Mice were euthanized, and metastatic nodules on liver were counted. Representative images and quantitative analysis of liver metastatic nodules were showed. Results represent the means ± SD from six mice. Data are shown as means ± SD and were analyzed by one-way ANOVA. $^{**}P < 0.01$; $^{***}P < 0.001$. n.s., not significant.

remain largely unexplored. In our study, MS analysis of BAP1-interacting proteins also identified UFL1, the key E3 enzyme in UFMylation, as a potential interactor of BAP1 (Fig. 2A). UFMylation is a recently discovered ubiquitin-like modification, although its substrates and functions in human cancers are not fully understood. We first validated the interaction between BAP1 and UFL1 in HCT116 cells using co-immunoprecipitation assay (Fig. 4A). Additionally, purified GST-BAP1, but not GST control, was able to bind to His-UFL1 in vitro (Fig. 4B). We also found that both full-length BAP1 (FL) and its N-terminal region (amino acids 1 to 240) could interact with UFL1 in vitro (fig. S4A).

Next, we investigated whether UFL1 could modify BAP1 through UFMylation. In cells cotransfected with components of the UFMylation machinery, including UBA5, UFC1, UFL1, UFM1 ΔC2 (an active form of UFM1), and UFBP1, UFMylation signaling was detected in anti–Flag-BAP1 immunoprecipitates, which displayed an additional 30-kDa molecular weight compared to UFMylation-free BAP1 (Fig. 4C). Similar results were obtained in an in vitro UFMylation assay (Fig. 4D). UFMylation of endogenous BAP1 can also be detected in CRC cells, and this modification was significantly reduced by UFL1 depletion (Fig. 4E). Further analysis revealed that UFMylation was present on the full-length and N-terminal region of BAP1 (amino acids 1 to 240), but not on the region spanning amino acids 241 to 729 (fig. S4B). To identify the specific lysing residues involved in BAP1 UFMylation, we mutated all 13 lysine residues within the N-terminal region (amino acids 1 to 240) to arginine. Single mutations at K51R, K61R, K187R, or K205R partially reduced BAP1 UFMylation (fig. S4C), while the simultaneous mutation of these four lysines 4KR almost completely abolished BAP1 UFMylation (Fig. 4F). Given the established direct interaction between BAP1 and pVHL, we next investigated whether

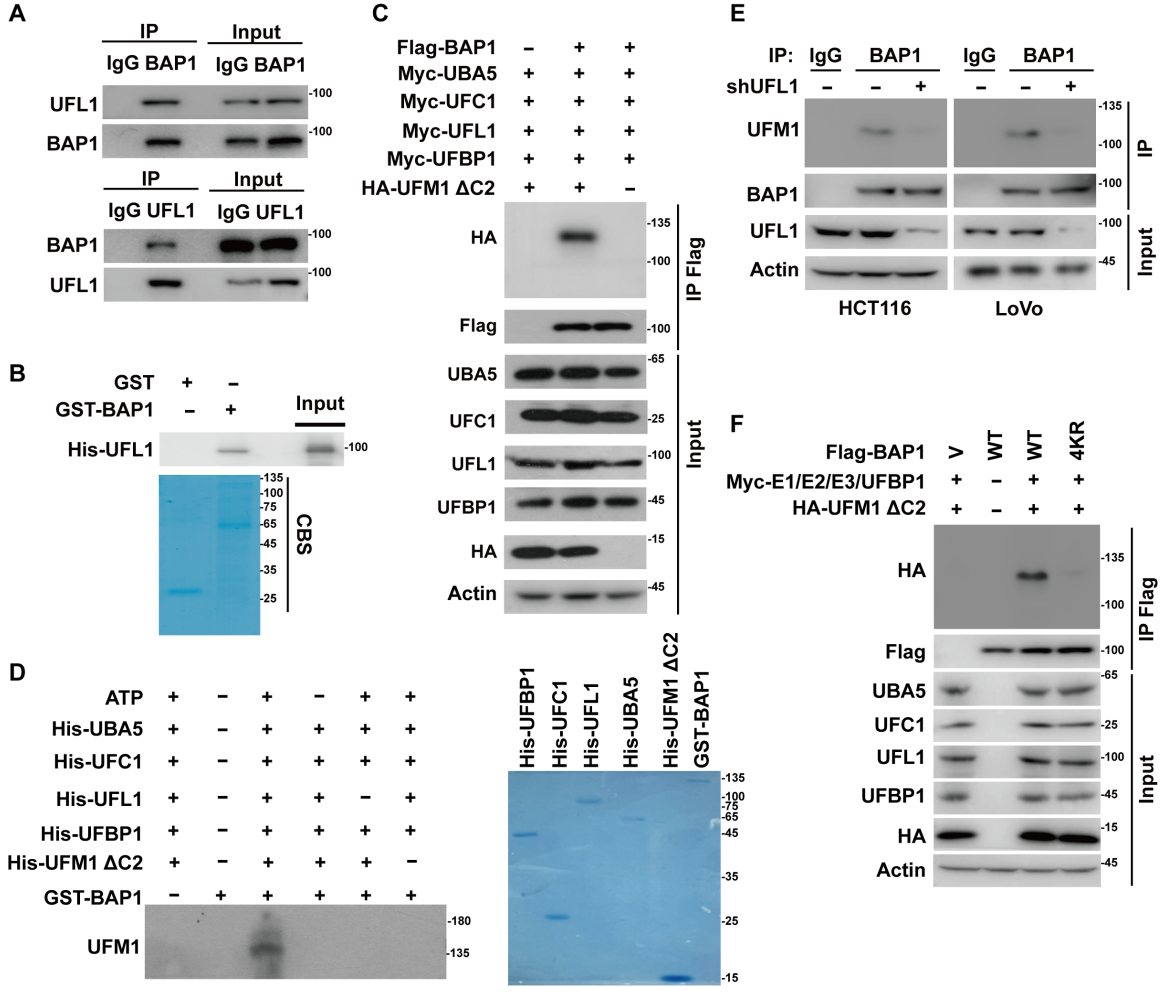

Fig. 4. UFL1 interacts with and UFMylates BAP1. (**A**) HCT116 cell lysates were subjected to immunoprecipitation with control IgG, anti-BAP1, or anti-UFL1 antibodies. The immunoprecipitates were then blotted with the indicated antibodies. (**B**) Purified recombinant GST, GST-BAP1, and His-UFL1 were incubated in vitro, and the direct interaction between BAP1 and UFL1 was examined. CBS, Coomassie blue staining. (**C**) UFMylation of BAP1 was analyzed by Western blotting using an anti-HA antibody in HEK293T cells transfected with Flag-BAP1 and the components of the UFMylation system (Myc-UBA5, Myc-UFC1, Myc-UFL1, Myc-UFBP1, and HA-UFM1 ΔC2). (**D**) In vitro UFMylation of BAP1. Purified UFMylation components (His-UBA5, His-UFC1, His-UFL1, His-UFBP1, and His-UFM1 ΔC2) were bacterially produced and incubated with GST or GST-BAP1 in UFMylation buffer at 30°C for 90 min. The reaction was stopped by the addition of SDS sample buffer containing 5% mercaptoethanol and boiled at 95°C for 10 min. Samples were subjected to Western blotting with an anti-UFM1 antibody. (**E**) UFMylation of endogenous BAP1 was analyzed by immunoprecipitation with an anti-BAP1 antibody, followed by Western blotting using an anti-UFM1 antibody in HCT116 and LoVo cells stably expressing control or UFL1 shRNA. (**F**) UFMylation assay of the Flag-BAP1 WT and 4KR was performed in HEK293T cells expressing the indicated components of the UFMylation system.

pVHL itself undergoes UFMylation. As shown in fig. S4D, no detectable UFM1 modification was observed on pVHL in cells co-transfected with Flag-S–tagged pVHL and components of the UFMylation machinery.

UFL1 regulates the stability and tumor-suppressive activity of pVHL in CRC

Given that UFL1 catalyzes the UFMylation of BAP1 and BAP1 stabilizes pVHL in CRC, we next investigated whether UFL1 also regulates pVHL stability and its tumor-suppressive activity. As shown in Fig. 5A and fig. S5A, depletion of UFL1 in CRC cells significantly decreased pVHL protein levels, while concurrently increasing HIF-1α levels. Notably, UFL1 depletion did not affect the expression of BAP1 or the mRNA levels of *VHL*. Consistent with these findings, pVHL protein was less stable in UFL1-deficient cells (Fig. 5B), likely due to the increased ubiquitination of pVHL (Fig. 5C). The instability of pVHL in UFL1-depleted cells may result from the impaired interaction between BAP1 and pVHL, while BAP1 interaction with other substrates, such as LKB1 and SLC7A11, remains unaffected (fig. S5B). UFL1 depletion did not alter the interaction between pVHL and the E3 ligase WSB1 (fig. S5C). In line with these observation, UFL1 depletion in CRC cells significantly enhanced cell proliferation, migration, and invasion while also decreasing cellular sensitivity to cisplatin and 5-FU both in vitro and in vivo. These effects were largely reversed by the reconstitution of Flag-VHL in UFL1-deficient cells (fig. S5, D to H).

UFL1 has previously been reported to compete with MDM2 to bind to WT p53, thereby stabilizing p53 (*37*). Given that the *TP53* gene is mutated or deficient in approximately half of human cancers, we next explored role of UFL1 in cancer cells with p53 loss or mutations. As shown in fig. S6 (A and B), the knockout (KO) of p53 in HCT116 or the knockdown of p53 in LoVo cells did not affect the ability of UFL1 to stabilize pVHL. Moreover, UFL1 depletion in p53-null AsPC-1 and p53-mutated SW620 cells markedly decreased pVHL protein levels without altering p53 expression (fig. S6, C and D). Intriguingly, reconstitution of pVHL in $p53^{-/-}$ HCT116, p53-depleted LoVo, p53-null AsPC-1, and p53-mutated SW620 cells almost completely abolished the increased cell proliferation induced by UFL1 depletion (fig. S6, E to H). These findings suggest that the tumor-suppressive activity of UFL1 is primarily mediated through the stabilization of pVHL, particularly in CRC cells with *P53* deficiency or mutations.

UFL1-mediated UFMylation activates BAP1 activity toward pVHL

We further investigated the mechanism by which UFL1 regulates pVHL turnover in CRC. As shown in Fig. 5D and fig. S6I, overexpression of UFL1 in HCT116 and LoVo cells increased pVHL protein level, which was mitigated by BAP1 knockdown. Additionally, UFL1 depletion reduced pVHL protein levels in control cells but did not further decrease pVHL levels in BAP1-deficient cells (Fig. 5E and fig. S6J), indicating that BAP1 is crucial for UFL1's regulation of pVHL stability. Moreover, overexpression of BAP1 WT markedly decreased the ubiquitination level of pVHL, and this effect was notably blocked by UFL1 depletion (Fig. 5F). These results suggest that UFL1 acts as a previously uncharacterized upstream regulator of BAP1-catalyzed deubiquitination of pVHL in CRC, influencing pVHL turnover and its associated tumor-suppressive functions.

We next examined the effects of UFL1-mediated UFMylation of BAP1 on pVHL stability and function. As shown in Fig. 5G and fig. S6K, reduced pVHL protein levels in BAP1-depleted cells could be largely rescued by reconstitution of BAP1 WT, but not the UFMylation-defective mutant 4KR. Consistently, reconstitution of BAP1, WT but not the 4KR mutant, markedly reduced the ubiquitination levels of pVHL and increased its half-life in endogenous BAP1-depleted cells (Fig. 5, H and I). This effect is likely due to the impaired interaction between pVHL and the BAP1 4KR mutant (Fig. 5J). To further elucidate the molecular mechanisms involved, we constructed a simulation model of ubiquitinated pVHL complexed with UFM1-conjugated BAP1. The structural predictions suggest that UFMylation of BAP1 generates additional interacting surfaces, enhancing its binding affinity to pVHL. Specifically, Arg^{15} and Tyr^{18} of K51-conjugated UFM1, along with Arg^{15} and Asp^{13} of K61-conjugated UFM1, form contacts with residues Arg^{161}, Val^{165}, and Ser^{168} on the H1 helix of pVHL, as well as Arg^{79}, Phe^{148}, and Asn^{150} on the β sheets of pVHL (fig. S6L and movie S1).

We also investigated the biological function of UFL1-mediated UFMylation of BAP1 in CRC. Reconstitution of BAP1 WT, but not the 4KR mutant, in endogenous BAP1-deficient HCT116 and LoVo cells significantly inhibited cell proliferation and sensitized cancer cells to cisplatin and 5-FU in vitro and in vivo (Fig. 5, K to M; and fig. S6, M and N). Furthermore, BAP1 WT reconstitution significantly suppressed the migration and invasion capabilities (fig. S6O) and reduced liver metastases compared to the 4KR mutant (Fig. 5N). These results demonstrate that UFL1-mediated UFMylation of BAP1 is critical for the stabilization and tumor-suppressive role of pVHL in CRC.

Correlations between UFL1, BAP1, and pVHL expression in clinical CRC samples

The clinical significance of the UFL1-BAP1-pVHL axis was further investigated in CRC specimens using both immunoblotting and IHC. As shown in Fig. 6 (A to C), the expression levels of UFL1 and pVHL were markedly reduced in most of CRC tumor samples compared to adjacent normal tissues. Notably, the down-regulation of UFL1 and BAP1 was positively correlated with reduced pVHL expression, respectively (Fig. 6D). Kaplan-Meier plot analysis revealed that lower levels of UFL1 or pVHL were notably associated with decreased overall survival in patients with CRC (fig. S7, A and B). Collectively, our findings underscore the pivotal role of UFL1-mediated UFMylation of BAP1 in stabilizing pVHL, thereby inhibiting CRC progression (Fig. 7A).

DISCUSSION

In this study, we reported several unexpected findings with potential clinical significance. We identify BAP1 as a previously unrecognized deubiquitinase for the key suppressor protein pVHL in CRC, facilitating pVHL stabilization and enhancing its tumor-suppressive function. Additionally, we uncover a previously unrecognized UFMylation-dependent mechanism that regulates BAP1 activity toward pVHL. Clinically, our histological analyses demonstrate that the down-regulation of UFL1 and BAP1 in CRC specimens is positively correlated with the decreased pVHL expression and associated with poor patient prognosis (Fig. 6, C and D). These findings underscore the crucial role of UFMylation in modulating the BAP1-pVHL–suppressive axis and suggest that targeting this pathway

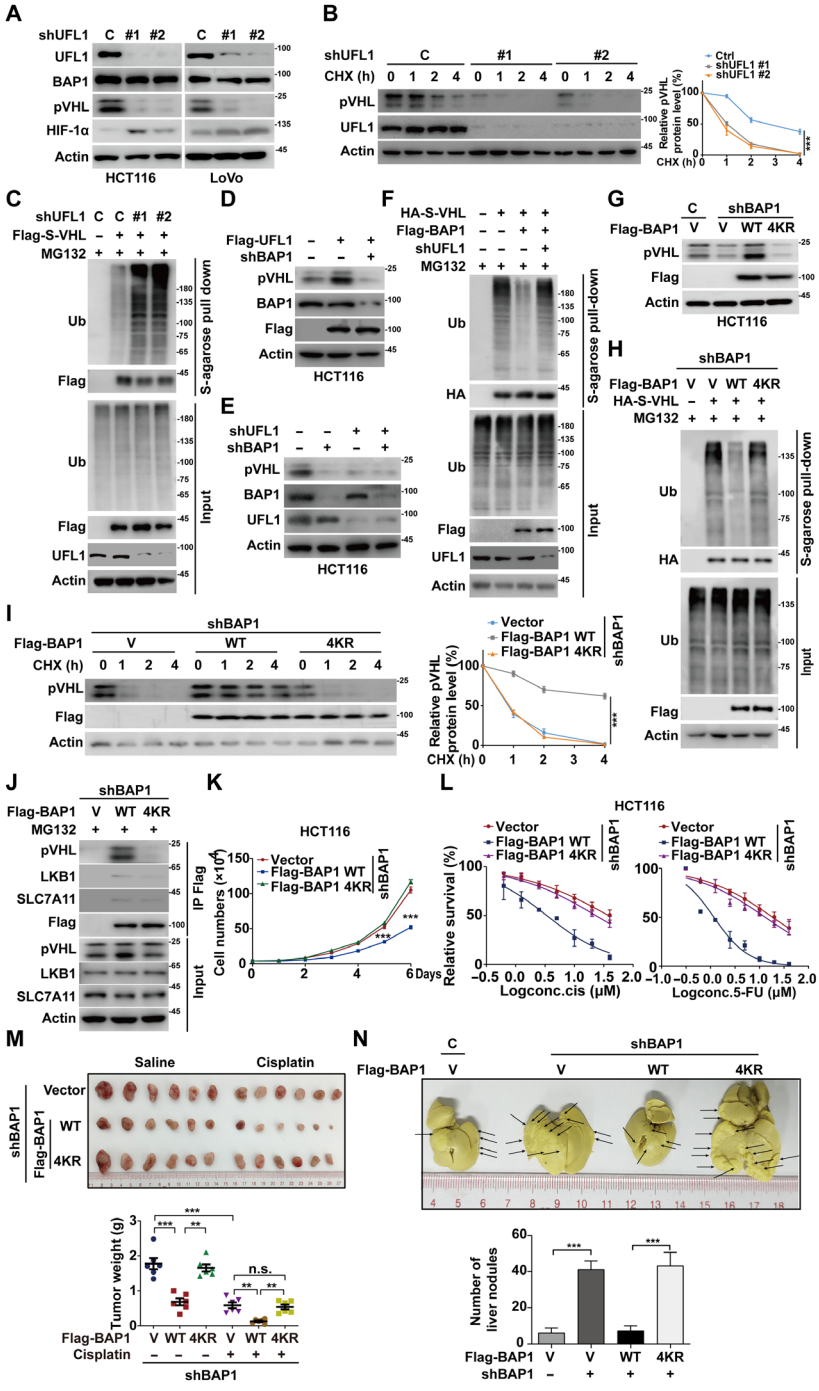

Fig. 5. UFL1-mediated UFMylation activates BAP1 activity toward pVHL in CRC. (**A**) Western blotting of HCT116 and LoVo cells stably expressing control or UFL1 shRNAs. (**B**) Cycloheximide pulse-chase assay from (A) assessing pVHL half-life (means ± SD, $n = 3$). (**C**) Cells from (A) were transfected with vector or pIRES-VHL (Flag/S tagged), treated MG132 for 10 hours, and subjected to S-agarose pull-down and anti-ubiquitin blotting. (**D**) HCT116 cells stably expressing Flag-UFL1 were infected with lentivirus expressing control or BAP1 shRNA. Western blot was performed. (**E**) Western blotting of HCT116 cells with BAP1, UFL1 or double knockdown using indicated antibodies. (**F**) Cells were transfected as indicated, followed by S-agarose pull-down and anti-ubiquitin blotting. (**G**) HCT116 cells were transfected with indicated plasmids, and Western blotting was performed. (**H**) Cells stably expressing BAP1 shRNA were transfected as indicated, treated MG132, and examined polyubiquitylated pVHL using an anti-ubiquitin antibody. (**I**) Cycloheximide pulse-chase assay in cells from (G) assessing pVHL half-life (means ± SD, $n = 3$). (**J**) Cells transfected as indicated were treated with MG132 and subjected to anti-Flag immunoprecipitation to assess BAP1 interaction with pVHL, LKB1, or SLC7A11. (**K**) Cell proliferation assays were performed on cells from (G) (means ± SD, $n = 3$). (**L**) Cells from (G) were treated with cisplatin or 5-FU, and cell survival was determined (means ± SD, $n = 4$). (**M**) HCT116 cells stably expressing vector, Flag-BAP1 WT, or 4KR mutant were injected subcutaneously into nude mice. Upon reaching about 100 mm^3, mice were treated with saline or cisplatin (2 mg/kg weekly, $n = 6$). Tumors were weighed at endpoint. n.s., not significant. (**N**) Cells as in (M) were injected into the spleen of nude mice. Metastatic nodules on liver were counted at endpoint. Results represent the means ± SD from six mice and were analyzed by one-way ANOVA. $^{**}P < 0.01$; $^{***}P < 0.001$. h, hours.

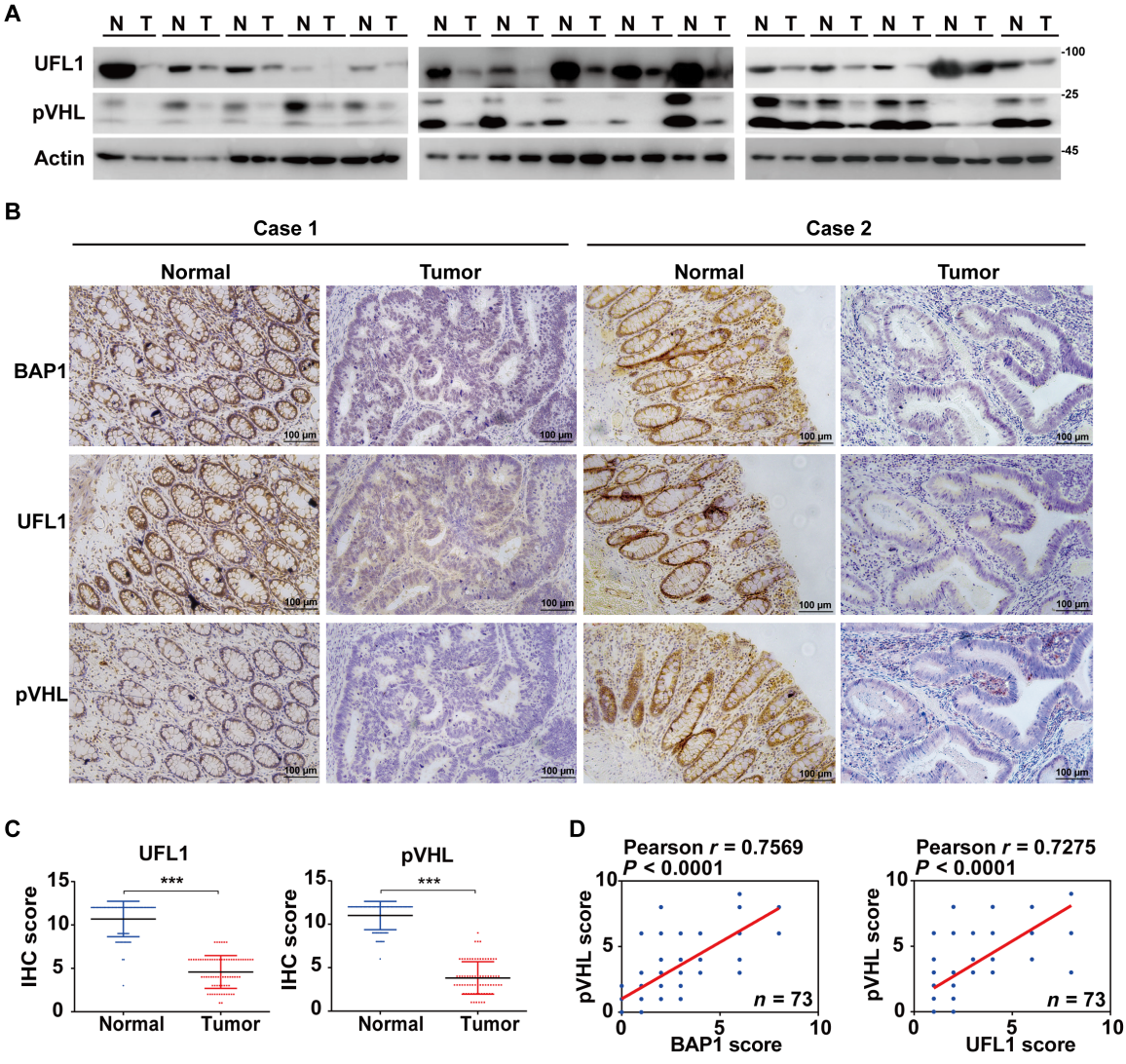

Fig. 6. BAP1 and UFL1 expressions are positively correlated with pVHL expression in CRC. (**A**) UFL1 and pVHL expressions in 15 pairs of fresh CRC tissues and adjacent normal tissues were measured by Western blotting. N, normal tissues; T, tumor tissues. (**B**) Representative IHC staining of BAP1, UFL1, and pVHL in CRC ($n = 73$) and adjacent normal tissues ($n = 73$). (**C**) The IHC scores of UFL1 and pVHL expression in (B) were analyzed. (**D**) The correlation of UFL1 and BAP1 expression with pVHL expressions in CRC tissues. Statistical analysis was performed with the chi-square test. *r*, the Pearson's correlation coefficient. Data are presented as the means ± SD and were analyzed by one-way ANOVA. ***$P < 0.001$.

could be a promising therapeutic strategy for CRC and potentially other cancers harboring WT *BAP1* and *VHL*.

Despite the well-established tumor-suppressing function of BAP1 in malignant mesothelioma, ccRCC, and uveal melanoma (*3*–*5*), the role and mechanism of BAP1 in CRC remains poorly understood. Kwon *et al.* reported that BAP1 is up-regulated in colon cancer cells and tissues and that BAP1 depletion reduces colon cancer cell proliferation and tumor growth (*38*). In contrast, two independent studies have shown that both mRNA and protein levels of BAP1 are down-regulated in most CRC tissues compared to adjacent non-cancerous tissues, with lower BAP1 expression being associated with shorter patient survival (*39*, *40*). In this study, we provide evidence supporting the tumor-suppressor role of BAP1 in CRC. First, analyses of the cBioPortal for Cancer Genomics databases reveal that the *BAP1* gene remains largely WT (fig. S1A). Second, overexpression of BAP1 WT, but not a catalytically inactive mutant C91S, significantly reduced cell proliferation, migration, and invasion. Additionally, BAP1 overexpression in CRC cells increased sensitivities to cisplatin and 5-FU, whereas BAP1 depletion has the opposite effects both in vitro and in vivo (Fig. 1, D to I; and fig. S1, D to G). Last, down-regulation of BAP1 expression was observed in primary CRC specimens, with an even more significant reduction in metastatic tissues compared to that in adjacent normal tissues, as demonstrated by immunoblotting and IHC analyses. This down-regulation correlates with poor clinical outcomes in patients with CRC (Fig. 1, B and C, and fig. S1C).

Notably, we reveal that the tumor-suppressive activity of BAP1 in CRC is primarily mediated through its interaction with the key suppressor protein pVHL, rather than previously reported substrates such as PTEN, LKB1, and SLC7A11, which are implicated in other

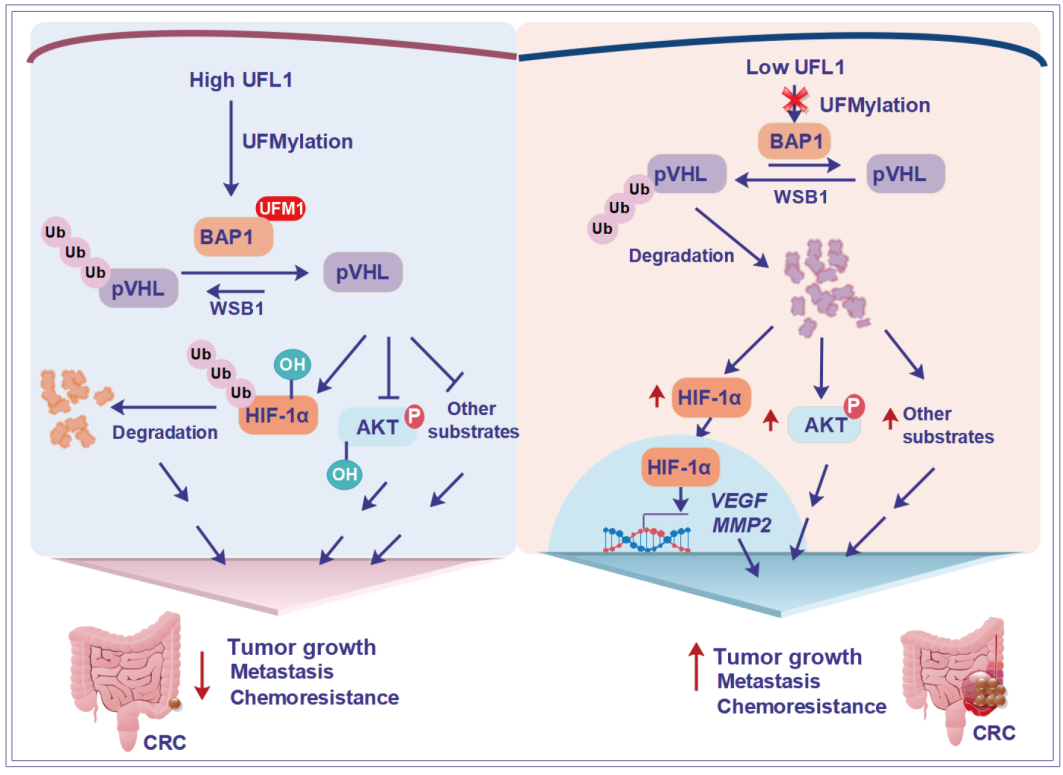

Fig. 7. The experimental model of this study. Schematic representation of the experimental model of this study, summarizing the proposed mechanisms by which UFL1-mediated UFMylation of BAP1 regulates pVHL stability and tumor-suppressive activity in CRC.

cancers (fig. S2A). pVHL, encoded by the *VHL* gene, functions as a tumor suppressor by acting as the substrate recognition component of the ubiquitin E3 ligase complex, targeting the degradation or inactivation of various substrates, including HIF-1α, HIF-2α, and Akt (*30*, *31*, *41*). Given the well-characterized tumor-suppressive activity of pVHL and its frequent down-regulation in cancers with WT *VHL*, stabilizing pVHL presents an appealing strategy for these cancers. However, as an unstable protein, pVHL undergoes ubiquitination and degradation by the ubiquitin E3 ligase WSB1, which has been showed to promote metastasis in melanoma (*35*). Although OTUD6B was reported to regulate pVHL stability in hepatocellular carcinoma, it acts as an adaptor protein that limits pVHL ubiquitylation by reducing its interaction with WSB1, independently of its deubiquitinase activity (*35*, *36*). To date, the bona fide deubiquitinase of pVHL has remained unidentified. Our study is the first, to our knowledge, to identify BAP1 as the previously uncharacterized deubiquitinase for pVHL, supported by several lines of evidence. First, BAP1 directly interacts with pVHL in cells and in vitro (Fig. 2, B and C). Second, BAP1 reduces pVHL ubiquitination through its deubiquitinating activity, leading to the stabilization of pVHL (Fig. 2, J and K). Third, genetic ablation of BAP1 significantly enhances cell proliferation, migration, invasion, and metastasis while also reducing CRC cells sensitivity to chemotherapies both in vitro and in vivo (Fig. 1, G to I; and fig. S1, E to G). Furthermore, reconstitution of pVHL significantly mitigated the phenotypes induced by BAP1 depletion in CRC cells, suggesting that the tumor-suppressive activity of BAP1 in CRC is largely dependent on its ability to stabilize pVHL (Fig. 3 and fig. S3, E, F, and I). Database analyses indicate that both *BAP1* and *VHL* are predominantly WTs in CRC (figs. S1A and S2B), and our findings demonstrate a strong clinical correlation between BAP1 and pVHL expression in CRC specimens (Fig. 6D). Additionally, the expression levels of both proteins are associated with patient prognosis in CRC (figs. S1C and S7, A and B). Collectively, these results underscore the potent tumor-suppressive role of BAP1 in CRC, primarily through the stabilization of pVHL.

The next critical question is how the activity of BAP1 toward pVHL is regulated in CRC. Various mechanism may play pivotal roles in regulating BAP1 expression across different cancers. While genetic alterations of the *BAP1* gene are frequently observed in cancers such as malignant pleural mesothelioma, ccRCC, and uveal melanoma, *BAP1* remains largely WT in CRC as evidenced by analyses of the cBioPortal for Cancer Genomics databases (fig. S1A). Our analysis of two independent human CRC scRNA-seq datasets (GEO: GSE132257 and GSE132465) and TCGA datasets revealed that the transcriptional level of *BAP1* are significantly lower in the epithelial tumor cells of CRC compared to normal tissues (Fig. 1A and fig. S1B). This suggests that transcriptional regulatory mechanism may play a role in modulating BAP1 expression. However, the specific mechanisms governing *BAP1* gene expression remain largely unexplored. Recent studies have reported that G-quadruplex (G4) structures in the *BAP1* promoter positively regulate its expression, while DNA helicases such as CHD7 can reduce *BAP1* promoter activity, likely by unwinding these G4 structures (*42*). CHD7 was amplified in more than 50% of CRC cases and is more highly expressed in tumor tissues than in adjacent normal

tissues, identifying it as a potential therapeutic target for CRC (*43*). Nonetheless, the underlying mechanisms and potential transcription factors involved in regulating *BAP1* transcription in CRC and other cancers remain to be fully elucidated.

In addition to transcriptional regulation, BAP1 is subject to various posttranslational modifications that modulate its stability and subcellular localization. For example, glutamylation of BAP1 at Glu^{651} by Tubulin Tyrosine Ligase-Like 5 (TTLL5) and Tubulin Tyrosine Ligase-Like 7 (TTLL7) promotes its ubiquitination and subsequent degradation, whereas CCP3 can remove this glutamylation, thereby stabilizing BAP1, enhancing Hoxa1 expression, and promoting the self-renewal of hematopoietic stem cells (*44*). Conversely, BAP1 undergoes multi-monoubiquitination catalyzed by the atypical E2/E3-conjugated enzyme UBE2O, leading to its sequestration in the cytoplasma and subsequent promotion of adipocyte differentiation (*17*). Additionally, BAP1 can be phosphorylated by multiple DNA damage-responsive kinases in response to genotoxic stress, facilitating its recruitment to sites of DNA double-strand breaks, where it regulates H2Aub levels and ensures the efficient assembly of DNA damage repair factors such as BRCA1 and RAD51 (*16*). Despite these insights, the mechanisms regulating BAP1's interaction with and activity toward its substrates remain largely unclear.

UFM1 is a recently identified ubiquitin-like modification that has emerged as a crucial posttranslational modification. Deficiency in UFMylation has been linked to anemia and murine embryonic lethality, underscoring its biological significance (*23*, *45*). Furthermore, UFMylation of histone H4 and MRE11 has been shown to promote ATM activation, highlighting its critical role in the DNA damage response (*46*, *47*). In our study, we identify UFMylation as a previously unrecognized posttranslational mechanism regulating BAP1 activity toward pVHL and its tumor-suppressive effects in CRC, based on several lines of evidence. First, UFL1, the E3 ligase responsible for UFMylation, directly interacts with BAP1 in CRC cells and in vitro (Fig. 4, A and B). Second, BAP1 is modified by mono-UFM1 at four lysine residues (Lys^{51}, Lys^{61}, Lys^{187}, and Lys^{205}) in its N-terminal region, both in vivo and in vitro (Fig. 4, C to E; and fig. S4, B and C). Notably, Lys^{187}, one of the UFMylation sites on BAP1, is also subject to ubiquitination (*17*). The interplay between these different posttranslational modifications that regulate BAP1 warrants further investigation. Third, UFL1-mediated UFMylation of BAP1 is crucial for its interaction with pVHL, facilitating the subsequent deubiquitination of pVHL and enhancing its tumor-suppressive effects in CRC (Fig. 5). The UFMylation sites within the catalytic domain of BAP1 (amino acids 1 to 240), which also serves as the interaction region with pVHL, are predicted by molecular dynamics (MD) simulations to alter the local structure or conformation of BAP1. These structural changes may create additional surfaces that interact with the H1 helix and β sheets of pVHL, thereby increasing BAP1's binding affinity to pVHL (fig. S6L and movie S1). Conversely, loss of UFMylation, either through UFL1 depletion or by reconstitution with the UFMylation-defective BAP1 mutant 4KR, markedly impairs the BAP1-pVHL interaction, leading to reduced stabilization of pVHL and a consequent loss of tumor-suppressive properties. In CRC cells, neither UFL1 depletion nor reconstitution of the 4KR mutant affected the weak interactions between BAP1 and other substrates, such as LKB1 and SLC7A11 (Fig. 5J and fig. S5B). This specific regulation of pVHL by BAP1 may be attributed to the unique additional binding interfaces formed between pVHL and UFMylated BAP1, which warrants further investigation.

Despite the critical role of UFMylation in stabilizing the BAP1-pVHL axis, translating this mechanism into therapeutic strategies faces challenges due to the pleiotropic nature of UFM1, which modifies multiple cellular proteins beyond BAP1. However, several features of the BAP1-UFL1 interaction identified in our study offer pathways to address specificity. First, while we observed that UFL1, the E3 ligase mediating UFMylation, is down-regulated in CRC (Fig 6), the upstream mechanisms regulating its transcription and protein stability in this context remain poorly characterized. A deeper understanding of these regulatory mechanisms may enable strategies to restore UFL1 expression, thereby enhancing BAP1 UFMylation and stabilizing pVHL. Nonetheless, we acknowledge that this approach would likely influence UFMylation globally, not exclusively that of BAP1. Second, a more selective strategy may involve enhancing the specific interaction between UFL1 and BAP1. For instance, high-throughput screening of Food and Drug Administration–approved drugs or other chemical libraries could identify small molecules that promote the UFL1-BAP1 interaction, thereby selectively enhancing BAP1 UFMylation. Additionally, the structural characterization of the UFL1-BAP1 complex will be instrumental in guiding such efforts and may uncover specific binding pockets or allosteric sites that could be targeted to modulate this interaction with higher specificity. Third, targeting the de-UFMylation process represents another potential strategy. Identifying enzymes responsible for de-UFMylation could potentially serve as a means to modulate BAP1 UFMylation levels. Ufm1-specific protease 2 (UFSP2) is now primary "de-UFMylation" enzyme for removing UFM1 modifications in human cells (*20*). Structural resolution of the potential BAP1-UFSP2 interface, combined with high-throughput compound screening, may enable the identification of inhibitors that disrupts such an interaction, thereby selectively enhancing BAP UFMylation by limiting its removal. Last, our MD simulations suggest that UFMylation of the catalytic domain of BAP1 (1 to 240 amino acids) induces conformational changes that enhances its interaction with the H1 helix and β sheets of pVHL (fig. S6L). This raises the possibility of designing allosteric modulators or mimetics that recapitulate the conformational effect of BAP1 UFMylation, potentially stabilizing BAP1 in an active configuration favorable for pVHL binding.

It is also noteworthy that we cannot rule out the possibility of additional mechanisms contributing to the suppressive activity of UFL1 in CRC, as ectopic expression of pVHL did not fully rescue functional alterations caused by UFL1 depletion in HCT116. A previous study reported that p53 can be UFMylated, which antagonizes MDM2-mediated ubiquitination, thereby maintaining p53 stability and its tumor-suppressive function in HCT116 cells (*37*). This suggests that UFL1-mediated UFMylation may stabilize both pVHL and p53 simultaneously, thereby suppressing cell proliferation in cancer cells harboring WT *TP53* and *VHL*, such as HCT116. Considering the frequent mutations and deletions of the *TP53* gene in human cancers, the stabilization of pVHL by the UFL1-BAP1 axis might be particularly important in cancer cells harboring *TP53* mutant or loss, such as CRC cells (SW620 and HCT116 with p53 KO) and pancreatic cancer cells (AsPC-1) (fig. S6, A to H). Intriguingly, Kaplan-Meier analysis indicated that high expressions of *UFL1* and *VHL* were associated with better overall survivals in CRC specimens harboring *TP53* mutant (fig. S7, A and B).

Collectively, our findings underscore the crucial role of UFMylation in modulating BAP1-mediated stabilization of pVHL in CRC. We

also confirmed that the BAP1-pVHL axis is applicable in pancreatic and ovarian cancer (fig. S3, G and H). However, further investigations are warranted to comprehensively characterize its role across different cancer types, particularly in the context of *TP53* mutations or deletions. These follow-up studies may provide deeper insights into the broader relevance of UFMylation and the UFL1-BAP1-pVHL axis in cancer biology and therapy.

MATERIALS AND METHODS

Cell culture, plasmids, and antibodies

Cell lines HCT116, LoVo, SW620, AsPC-1, MIA PaCa-2, A2780, SKOV3, and human embryonic kidney (HEK) 293T were purchased from American Type Culture Collection. HCT116 p53 WT and p53 KO cells were provided by J. Zhang from Kunming University of Science and Technology. Cell lines were mycoplasma free and authenticated by short tandem repeat DNA profiling analysis. HCT116 cells were cultured in McCoy's 5A medium. AsPC-1 cells were cultured in RPMI 1640 medium with 10% fetal bovine serum (FBS). LoVo cells were cultured in F-12 K medium with 10% FBS. MIA PaCa-2, A2780, SKOV3, and HEK293T cells were cultured in Dulbecco's modified Eagle's medium (DMEM) with 10% FBS. The cell incubator contained 5% CO_2 and maintained a constant temperature and humidity environment at 37°C. SW620 cells were cultured in Leibovitz's L-15 medium with 10% FBS at 37°C without CO_2.

Plasmids BAP1, VHL, and UFL1 were cloned into pIRES-Flag-S, pLV.3-Flag, pLV.3-Flag-S, pLV.5-HA-S, pET28a, and pGEX4T-1 vectors. All site mutants were generated by site-directed mutagenesis and identified by sequencing. For the overexpression experiments, the empty vectors were used as a negative control.

Antibodies anti-BAP1 (C-4) (sc-28383; dilution, 1:1000), anti-Myc (9E10; dilution, 1:1000), anti-WSB1 (sc-393200; dilution, 1:500), and anti-Ubiquitin (Ub) (sc-8017; dilution, 1:1000) antibodies were purchased from Santa Cruz Biotechnology. Anti-Flag (F1804; dilution, 1:1000), anti-HA (H3663; dilution, 1:1000), and anti–β-actin (A1978; dilution, 1:5000) antibodies were purchased from Sigma-Aldrich. Anti-VHL (68547; dilution, 1:1000), anti-p53 (2527S; dilution, 1:1000), anti-PTEN (138G6; dilution, 1:1000), anti-LKB1 (D60C5; dilution, 1:1000), anti-SLC7A11 (D2M7A; dilution, 1:1000), anti–p-AKT (Ser^{473}) (4060S; dilution, 1:1000), anti-K48 or K63-linkage–specific polyubiquitin (8081 or 5621; dilution, 1:1000), and anti-cleaved caspase-3 (9664S; dilution, 1:200) antibodies were purchased from Cell Signaling Technology. Anti-Ki67 (SR00-02; dilution, 1:200) antibody was purchased from HUABIO. Anti-UFM1 (ab109305; dilution, 1:1000) antibodies were purchased from Abcam. Anti-UFL1 (A303-456A; dilution, 1:1000) and anti–HIF-1α (A300-286A; dilution, 1:500) antibodies were purchased from BETHYL. Heavy or light-chain–specific IPKine horseradish peroxidase (Abbkine Scientific Co.; A25222 and A25012) were used in co-immunoprecipitation experiment.

RNA interference

In short hairpin RNA (shRNA) experiments, pLKO.1-scramble shRNA was used as a negative control with the sequence of CCTAAGGTTAAGTCGCCCTCG. The shRNA targeting sequences for BAP1 shRNA #1 and #2 are 5′-CGTCCGTGATTGATGATGATA-3′ and 5′-CCACAACTACGATGAGTTCAT-3′, respectively. The shRNA targeting sequences for UFL1 shRNA #1 and #2 are 5′-GCTCTGGAACATGGGTTGATA-3′ and 5′-GAAACACTTCTGTGTCAGAAA-3′, respectively. The shRNA targeting sequences for VHL shRNA #1 and #2 are 5′-CCCTATTAGATACACTTCTTA-3′ and 5′-GCCTAGTCAAGCCTGAGAATT-3′.

Quantitative real-time polymerase chain reaction

Cultured cell RNA isolation was carried out using TRIzol reagent (Thermo Fisher Scientific, MA, USA). Subsequent conversion of the extracted RNA into cDNA was achieved via a FastKing gDNA Dispelling RT SuperMix kit (Tiangen, Beijing, China). Quantitative real-time polymerase chain reaction (qRT-PCR) analysis was performed using FastFire qPCR PreMix (SYBR Green) as described previously (*48*). All experiments were performed in triplicate with glyceraldehyde-3-phosphate dehydrogenase (GAPDH) as an internal control. Primer sequences are listed as follows: *VHL*: (forward) CTGCCCGTATGGCTCAACTT and (reverse) GTGTGTCCCTGCATCTCTGAA; *MMP2*: (forward) TGACTTTCTTGGATCGGGTCG and (reverse) AAGCACCACATCAGATGACTG; *VEGF*: (forward) GAGGAGCAGTTACGGTCTGTG and (reverse) TCCTTTCCTTAGCTGACACTTGT; and *GAPDH*: (forward) GATCGAATTAAACCTTATCGTCGT and (reverse) GCAGCAGAACTTCCACTCGGT.

Western blotting analysis

Whole-cell lysates were prepared by sonication in NETN buffer [20 mM tris-HCl (pH 8.0), 300 mM NaCl, 1 mM EDTA, and 0.5% NP-40] containing 1× protease inhibitor cocktail (Roche), 10 mM β-glycerophosphate, 1 mM sodium orthovanadate, 10 mM sodium fluoride, and 1 mM phenylmetnylsulfonyl fluoride. Proteins were separated by SDS–polyacrylamide gel electrophoresis gel electrophoresis and transferred to polyvinylidene difluoride membranes and then incubated with the primary and secondary antibodies.

CCK-8 assay

A Cell Counting Kit-8 (CCK-8; HY-K0301) was used to measure the survival of HCT116 and LoVo cells as described previously (*48*). Cells were seeded at a density of 2000 cells per well in 96-well plates. A total of 2000 cells in a volume of 100 μl per well were cultured in four replicate wells in a 96-well plate in medium containing 10% FBS. Cells were treated with different concentrations of Cisplatin or 5-FU for 72 hours, and CCK-8 reagent (15 μl) was added and incubated for 2 hours.

Migration and invasion assays

Cells (8000 to 10,000 per well) stably expressing indicated constructs were resuspended in serum-free DMEM for inoculation onto the membranes of 24-well transwell inserts (pore size, 8 mm; Corning, NY, USA) in the upper chamber. Inserts with non-coated membranes were used for migration assay, while inserts with Matrigel-coated membranes were used for invasion assay. DMEM containing 20% FBS served as chemoattractant in the lower chambers. After culturing for 48 hours, cells that migrated or invaded to the surface of lower chambers were fixed and stained with crystal-violet and counted in five randomly selected microscopic fields (*48*).

Immunoprecipitation

Immunoprecipitation was performed as described previously (*48*). HCT116 cells were lysed in NETN buffer and were incubated overnight with primary antibodies together with protein A/G beads (Thermo Fisher Scientific) for 2 hours at 4°C. After washing for five times, immunoprecipitates were subjected to Western blotting. HCT116 and HEK293T cells transfected as indicated were lysed in NETN buffer

and were incubated at 4°C with anti-Flag affinity gel (Sigma-Aldrich) or S-agarose (Merck Millipore) for 4 hours. The immunoprecipitates were subjected to Western blotting.

GST pull-down assay

Indicated cDNA was cloned into pGEX4T-1 or pET28a vector and transfected into *Escherichia coli* strain BL21. After the induction by 200 μM isopropyl-β-D-thiogalactopyranoside (IPTG) (Sigma-Aldrich, I6758-1G) for overnight, at 18°C, GST or GST-fusion proteins were purified by using Pierce Glutathione Agarose (Thermo Fisher Scientific). Purified GST or GST-BAP1 protein bound to Pierce Glutathione Agarose was incubated with His-VHL or His-UFL1 for 2 hours at 4°C. Beads were then washed with NETN buffer for four times, followed by Western blotting.

Denaturing immunoprecipitation for ubiquitination

Denaturing immunoprecipitation for ubiquitination was performed as described previously (*49*). Cells were treated with MG132 for 10 hours before harvest. Then, cells were lysed in 100 μl of 62.5 mM tris-HCl (PH 6.8), 2% SDS, 10% glycerol, 20 mM NEM, and 1 mM iodoacetamide; boiled at 95°C for 15 min and then diluted 10 times with NETN buffer containing protease inhibitors, 20 mM NEM, and 1 mM iodoacetamide; and centrifuged to remove cell debris. Proteins were immunoprecipitated with indicated antibodies and blotted with indicated antibody.

In vitro deubiquitination assay

In vitro deubiquitination assay was performed as described previously (*50*). *E. coli* strain BL21 and Pierce Glutathione Agarose were used to express and purify recombinant GST-fused BAP1 WT and C91S (CS) mutant protein. HCT116 cells were transfected with empty vector or HA-S-VHL followed with the treatment of MG132 (10 μM) for 10 hours. pVHL was pulled down by S-agarose and then incubated with purified GST-BAP1 WT or C91S fusion protein for 4 hours. Western blotting was performed to analyze the ubiquitination of pVHL.

UFMylation assay in vivo and in vitro

In vivo UFMylation assay

HEK293T cells were transfected with BAP1 constructs and the UFMylation system components (Myc-UBA5, Myc-UFC1, Myc-UFL1, Myc-UFBP1, and HA-UFM1 ΔC2). For the detection of endogenous BAP1 UFMylation, HCT116 and LoVo cells were treated with MG132 (10 μM) for 10 hours before harvesting. Forty-eight hours later, cells were lysed by boiling in buffer [150 mM tris-HCl (pH 8), 5% SDS, and 30% glycerol] for 10 min. Cell lysates were diluted 20-fold with buffer A [50 mM tris-HCl (pH 8), 150 mM NaCl, 10 mM imidazole, 1% Triton X-100 or 0.5% NP-40, 1× protease inhibitor cocktail, and 2 mM NEM] as described previously (*37*) and immunoprecipitated with indicated antibodies. Western blot was performed to measure the UFMylation level of immunoprecipitated proteins.

In vitro UFMylation assay

Indicated proteins were purified as previously described (*47*). Briefly, GST-BAP1 was ectopically expressed in *E. coli* strain BL21, induced by IPTG, and purified using Glutathione Sepharose. His-UBA5, His-UFC1, His-UFL1, His-UFBP1 and His-UFM1 ΔC2 were expressed in *E. coli* strain BL21 cells, induced by IPTG, and purified using Ni–nitrilotriacetic acid agarose (QIAGEN). Purified His-UBA5 (0.1 μM), His-UFC1 (0.1 μM), His-UFL1 (0.1 μM), His-UFBP1 (0.1 μM), His-UFM1 ΔC2 (0.1 μM), and GST-BAP1 (0.1 μM) were mixed in a reaction buffer [0.05% bovine serum albumin and 50 mM Hepes (pH 7.5)] containing 5 mM adenosine 5′-triphosphate and 10 mM $MgCl_2$ and incubated at 30°C for 90 min. The mixtures were boiled with the addition of SDS sample buffer containing 5% mercaptoethanol for 10 min.

MD simulations

The ubiquitinated VHL/BAP1-UFM1 complex is modeled using maestro (Schrödinger, LLC, New York, NY, USA, 2023). The structure of ubiquitin and BAP1 were retrieved from the BAP1-ASXL1 complex bound to chromatosome [Protein Data Bank (PDB) ID: 8H1T]. The Gly^{76} of ubiquitin was conjugated to Lys^{171} of VHL (PDB ID: 1VCB). The structure of UFM1 was retrieved from PDB ID: 5HKH and conjugated to Lys^{51}, Lys^{61}, Lys^{187}, and Lys^{205} of BAP1. OPLS4 force filed was used, and MD simulation was performed using Desmond. The system was relaxed for 5 ns before 500-ns production simulations, and the simulations were conducted in isothermal-isobaric ensemble (NPT ensemble) at 300 K and 1 atm using default settings.

Tandem affinity purification and MS analyses

Protein purification and MS analysis were conducted following established protocols (*48*). In brief, tandem affinity purification in cells expressing Flag-S empty vector, Flag-S-BAP1 was conducted by combining Flag-tag purification with anti-Flag affinity gel (first purification) followed by the immunoprecipitation with the S-agarose (second purification). HCT116 cells were transfected with Flag-S–tagged empty vector, Flag-S-BAP1. Cells were treated with MG132 (10 μM) for 10 hours, and cell pellets were then collected and lysed in NETN buffer (pH 8.0, 300 mM NaCl, 20 mM tris-HCl, 0.5% NP-40, and 1 mM EDTA) containing protease inhibitors [1× protease inhibitor cocktail (Roche), 1 mM sodium orthovanadate, 10 mM β-glycerophosphate, 1 mM phenylmetnylsulfonyl fluoride, and 10 mM sodium fluoride]. Anti-Flag Affinity Gel (20 μl; Sigma-Aldrich) was added into cell lysates and rotated at 4°C for 2 hours. Anti-Flag immunoprecipitates were washed three times with cold NETN buffer and incubated with 100 μl of 3× Flag peptide working solution at the concentration of 100 μg/ml (Sigma-Aldrich, F4799) at 4°C for 2 hours. The elution process was repeated for three additional times, and the combination of elutes was diluted by NETN buffer. For the second purification step, 50 μl of S-agarose (Merck Millipore) was added into the diluted elutes and incubated at 4°C for 4 hours. The immunoprecipitates by S-agarose were washed by NETN buffer for three times. The beads were resuspended in 500 μl of 6 M urea in phosphate-buffered saline (PBS), 25 μl of 200 mM dithiothreitol in 25 mM NH_4HCO_3 buffer was added, and the reaction was incubated at 37°C for 30 min. For alkylation, 25 μl of 400 mM indole-3-acetic acid in 25 mM NH_4HCO_3 buffer was added, followed by incubation for 30 min at room temperature in dark. The supernatant was then removed, and the beads were washed with 1 ml of PBS once. For the digestion, 150 μl of 2 M urea in PBS, 150 μl of 1 mM $CaCl_2$ in 50 mM NH_4HCO_3, and 1 μl of trypsin (1.0 μg/μL) were added. The reaction was incubated at 37°C overnight. The peptides were collected by washing three times with 200 μl of water, and then the peptides were desalted by C18 column. After evaporation in SpeedVac, the samples were tested by liquid chromatography–tandem MS (MS/MS), equipped with an EASY-nLC 1200 HPLC system and Orbitrap Fusion Lumos mass spectrometer (Thermo Fisher Scientific). The raw data were processed by using Proteome Discoverer

2.5 and processed as per default workflow. MS tolerance is 4.5 parts per million (ppm), and MS/MS tolerance is 20 ppm. Searches were performed against the *Homo sapiens* UniProt canonical 20395 entries 20210516 nm fasta. Reversed database searches were used to evaluate false discovery rate of site, peptide, and protein identifications. Two missed cleavage sites of trypsin were allowed. Protein hits were refined by corresponding volcano plots as $\log_2$ fold change of Flag-S-BAP1/empty vector against statistical significance ($-\log_{10}$ *P* value). Protein hits with $\log_2$ fold change of BAP1/empty vector larger than 2 and $-\log_{10}$ *P* value larger than 1.35 in mass spectrum experiments were further considered.

RNA-seq analysis

The RNA-seq experiment was performed by Shanghai OE Biotech, as previously described (*51*). Total RNA was extracted using the TRIzol reagent (Invitrogen, CA, USA). RNA purity and quantification were evaluated using the NanoDrop 2000 spectrophotometer (Thermo Fisher Scientific, USA). RNA integrity was assessed using the Agilent 2100 Bioanalyzer (Agilent Technologies, Santa Clara, CA, USA). Then, the libraries were constructed using the VAHTS Universal V10 RNA-seq Library Prep Kit (Premixed Version) according to the manufacturer's instructions. The transcriptome sequencing and analysis were conducted by OE Biotech Co. Ltd. (Shanghai, China).

Gene set enrichment analysis (GSEA) was performed using GSEA software. The analysis was used a predefined gene set, and the genes were ranked according to the degree of differential expression in the two types of samples. Then, it is tested whether the predefined gene set was enriched at the top or bottom of the ranking list.

Kaplan-Meier survival analysis

Kaplan-Meier survival analysis was performed using the Kaplan-Meier Plotter online tool (http://kmplot.com) to evaluate the prognostic significance of *BAP1*, *UFL1*, and *VHL* in CRC. The survival curves and corresponding hazard ratios were calculated based on default settings. The analysis was conducted as previously described (*52*).

Tumor xenograft assay in vivo

For subcutaneous xenografting, HCT116 cells (1×10^6) were resuspended in 100 μl of PBS and inoculated subcutaneously in the flanks of 4- to 6-week-old female BALB/c-nude mice. Tumor volume was measured every 2 days by using a vernier caliper to measure the long diameter and short diameter of the tumor and calculated as follows: $V = a$ (short diameter)$^2 \times b$ (long diameter) $\times 0.4$ (*48*). When tumor volume reached 100 mm^3, mice were randomly divided into two groups and receive intraperitoneal injections of saline or cisplatin (2 mg/kg) once a week ($n = 6$). Six weeks later, mice were euthanized, and tumor weight was measured. For the liver metastasis study, HCT116 cells (5×10^6) were transfected as indicated and injected into the spleen of 4- to 6-week-old female nude mice ($n = 6$). Mice were euthanized after 30 days, and the number of metastatic liver nodules was counted and quantified. The experiment protocol was approved by the Institutional Animal Care and Use Committee (IACUC) in Jinan University (20220219-05).

CRC patient-derived xenograft model

PDXs were provided by C. Shan (Nankai University). PDX model was established according to the previous studies (*50*, *53*). Briefly, CRC PDXs were cut into pieces of 3 mm by 3 mm by 3 mm using sterile surgical instruments, and tumor blocks were inserted into the back of mice by inoculation needle. Tumor volumes were measured three times weekly by using a vernier caliper. For lentivirus injection, lentiviruses were produced in HEK293T cells transfected with control, BAP1 shRNA, BAP1 shRNA plus Flag-VHL or UFL1 shRNA, and UFL1 shRNA plus Flag-VHL. Then, viruses were filtered through a 0.45-μm filter and concentrated using PEG 8000 precipitation. When tumor volumes reached 30 mm^3, the center of the xenograft tumors were intratumorally injected three times with the indicated lentivirus (1×10^8 plaque-forming units/100 μl per mouse) to knockdown endogenous BAP1 or UFL1. When tumor volumes reached 100 mm^3, mice were administered saline or cisplatin (2 mg/kg) once a week ($n = 6$). Mice were euthanized at the indicated time and tumor weights were measured. All animal experiments were performed in accordance with a protocol approved by the IACUC in Jinan University (20230329-22).

Immunohistochemical staining

CRC pathological tissue sections were obtained from the tissue bank at the First Affiliated Hospital of Jinan University in accordance with the approval document of the Institutional Medical Ethics Committee (ethics approval license: JNUKY-2022-098). IHC assays were conducted on paraffin-embedded specimens of patients with CRC using anti-pVHL, anti-BAP1, or anti-UFL1 antibodies, respectively. The immunostaining was blindly scored by two pathologists. The IHC score was calculated by combining the quantity score (percentage of positively stained tissues) with the staining intensity score. The score for each tissue was calculated by multiplying the quantity with the intensity score (the range of this calculation was therefore 0 to 12). An IHC score of 9 to 12 was considered a strong immunoreactivity; 5 to 8, moderate; 1 to 4, weak; and 0, negative. Samples with IHC score > 4 were considered to be high and ≤ 4 were considered to be low. The chi-square test and the Pearson's correlation coefficient were used for statistical analysis of the correlation between pVHL and BAP1 or UFL1. In tumors from animal experiments, hematoxylin and eosin (H&E) and immunostaining of Ki67 and cleaved caspase-3 were performed. In brief, tumors samples were fixed with 4% paraformaldehyde, embedded in paraffin, and microtome sliced into 5-μm sections. Following dewaxing and dehydrating, anti-Ki67 (dilution, 1:200) and cleaved caspase-3 (dilution, 1:200) antibodies were used for immunohistochemical staining of tumor sections from mice. H&E staining of the slides was performed according to the manufacturer's instructions (E607318, Sangon Biotech). Slices were then imaged using a microscope (Olympus) (*48*).

Statistical analysis

All data are analyzed by GraphPad Prism 5.0 software. Each experiment was performed at least three times, following the principle of repeatability. The experimental data represent the means ± SD. The differences between two groups of data were compared using *t* test, and the differences between multiple groups of data were compared using one-way analysis of variance (ANOVA) and Tukey's test: compare all pairs of columns. $P < 0.05$ is considered to be statistically significant.

Supplementary Materials

The PDF file includes:

Figs. S1 to S7
Legend for movie S1
Legend for data S1

Other Supplementary Material for this manuscript includes the following:
Movie S1
Data S1

REFERENCES AND NOTES

1. H. Sung, J. Ferlay, R. L. Siegel, M. Laversanne, I. Soerjomataram, A. Jemal, F. Bray, Global cancer statistics 2020: GLOBOCAN estimates of incidence and mortality worldwide for 36 cancers in 185 countries. *CA Cancer J. Clin.* **71**, 209–249 (2021).
2. H. Zhou, Z. Liu, Y. Wang, X. Wen, E. H. Amador, L. Yuan, X. Ran, L. Xiong, Y. Ran, W. Chen, Y. Wen, Colorectal liver metastasis: Molecular mechanism and interventional therapy. *Signal Transduct. Target. Ther.* **7**, 70 (2022).
3. J. R. Testa, M. Cheung, J. Pei, J. E. Below, Y. Tan, E. Sementino, N. J. Cox, A. U. Dogan, H. I. Pass, S. Trusa, M. Hesdorffer, M. Nasu, A. Powers, Z. Rivera, S. Comertpay, M. Tanji, G. Gaudino, H. Yang, M. Carbone, Germline BAP1 mutations predispose to malignant mesothelioma. *Nat. Genet.* **43**, 1022–1025 (2011).
4. M. Gerlinger, S. Horswell, J. Larkin, A. J. Rowan, M. P. Salm, I. Varela, R. Fisher, N. McGranahan, N. Matthews, C. R. Santos, P. Martinez, B. Phillimore, S. Begum, A. Rabinowitz, B. Spencer-Dene, S. Gulati, P. A. Bates, G. Stamp, L. Pickering, M. Gore, D. L. Nicol, S. Hazell, P. A. Futreal, A. Stewart, C. Swanton, Genomic architecture and evolution of clear cell renal cell carcinomas defined by multiregion sequencing. *Nat. Genet.* **46**, 225–233 (2014).
5. J. W. Harbour, M. D. Onken, E. D. Roberson, S. Duan, L. Cao, L. A. Worley, M. L. Council, K. A. Matatall, C. Helms, A. M. Bowcock, Frequent mutation of BAP1 in metastasizing uveal melanomas. *Science* **330**, 1410–1413 (2010).
6. S. Perkail, J. Andricovich, Y. Kai, A. Tzatsos, BAP1 is a haploinsufficient tumor suppressor linking chronic pancreatitis to pancreatic cancer in mice. *Nat. Commun.* **11**, 3018 (2020).
7. Y. Zhang, J. Shi, X. Liu, L. Feng, Z. Gong, P. Koppula, K. Sirohi, X. Li, Y. Wei, H. Lee, L. Zhuang, G. Chen, Z. D. Xiao, M. C. Hung, J. Chen, P. Huang, W. Li, B. Gan, BAP1 links metabolic regulation of ferroptosis to tumour suppression. *Nat. Cell Biol.* **20**, 1181–1192 (2018).
8. X. X. Chen, Y. Yin, J. W. Cheng, A. Huang, B. Hu, X. Zhang, Y. F. Sun, J. Wang, Y. P. Wang, Y. Ji, S. J. Qiu, J. Fan, J. Zhou, X. R. Yang, BAP1 acts as a tumor suppressor in intrahepatic cholangiocarcinoma by modulating the ERK1/2 and JNK/c-Jun pathways. *Cell Death Dis.* **9**, 1036 (2018).
9. L. Wang, N. W. Birch, Z. Zhao, C. M. Nestler, A. Kazmer, A. Shilati, A. Blake, P. A. Ozark, E. J. Rendleman, D. Zha, C. A. Ryan, M. A. J. Morgan, A. Shilatifard, Epigenetic targeted therapy of stabilized BAP1 in ASXL1 gain-of-function mutated leukemia. *Nat. Cancer* **2**, 515–526 (2021).
10. S. Asada, S. Goyama, D. Inoue, S. Shikata, R. Takeda, T. Fukushima, T. Yonezawa, T. Fujino, Y. Hayashi, K. C. Kawabata, T. Fukuyama, Y. Tanaka, A. Yokoyama, S. Yamazaki, H. Kozuka-Hata, M. Oyama, S. Kojima, M. Kawazu, H. Mano, T. Kitamura, Mutant ASXL1 cooperates with BAP1 to promote myeloid leukaemogenesis. *Nat. Commun.* **9**, 2733 (2018).
11. A. P. Szczepanski, Z. Zhao, T. Sosnowski, Y. A. Goo, E. T. Bartom, L. Wang, ASXL3 bridges BRD4 to BAP1 complex and governs enhancer activity in small cell lung cancer. *Genome Med.* **12**, 63 (2020).
12. N. Tsuboyama, R. Wang, A. P. Szczepanski, H. Chen, Z. Zhao, L. Shi, L. Wang, Therapeutic targeting of BAP1/ASXL3 sub-complex in ASCL1-dependent small cell lung cancer. *Oncogene* **41**, 2152–2162 (2022).
13. J. Qin, Z. Zhou, W. Chen, C. Wang, H. Zhang, G. Ge, M. Shao, D. You, Z. Fan, H. Xia, R. Liu, C. Chen, BAP1 promotes breast cancer cell proliferation and metastasis by deubiquitinating KLF5. *Nat. Commun.* **6**, 8471 (2015).
14. C. Yang, H. Ding, Y. Yang, L. Yang, Y. Yang, M. Fang, J. Ren, R. Hu, C. Wang, W. Geng, BAP1 regulates AMPK-mTOR signalling pathway through deubiquitinating and stabilizing tumour-suppressor LKB1. *Biochem. Biophys. Res. Commun.* **529**, 1025–1032 (2020).
15. I. H. Ismail, R. Davidson, J. P. Gagné, Z. Z. Xu, G. G. Poirier, M. J. Hendzel, Germline mutations in BAP1 impair its function in DNA double-strand break repair. *Cancer Res.* **74**, 4282–4294 (2014).
16. H. Yu, H. Pak, I. Hammond-Martel, M. Ghram, A. Rodrigue, S. Daou, H. Barbour, L. Corbeil, J. Hebert, E. Drobetsky, J. Y. Masson, J. M. Di Noia, E. B. Affar, Tumor suppressor and deubiquitinase BAP1 promotes DNA double-strand break repair. *Proc. Natl. Acad. Sci. U.S.A.* **111**, 285–290 (2014).
17. N. Mashtalir, S. Daou, H. Barbour, N. N. Sen, J. Gagnon, I. Hammond-Martel, H. H. Dar, M. Therrien, E. B. Affar, Autodeubiquitination protects the tumor suppressor BAP1 from cytoplasmic sequestration mediated by the atypical ubiquitin ligase UBE2O. *Mol. Cell* **54**, 392–406 (2014).
18. T. J. Yang, T. N. Li, R. S. Huang, M. Y. Pan, S. Y. Lin, S. Lin, K. P. Wu, L. H. Wang, S. D. Hsu, Tumor suppressor BAP1 nuclear import is governed by transportin-1. *J. Cell Biol.* **221**, e202201094 (2022).
19. Y. Gerakis, M. Quintero, H. Li, C. Hetz, The UFMylation system in proteostasis and beyond. *Trends Cell Biol.* **29**, 974–986 (2019).
20. Y. Wei, X. Xu, UFMylation: A unique & fashionable modification for life. *Genomics Proteomics Bioinformatics* **14**, 140–146 (2016).
21. Y. Cai, N. Singh, H. Li, Essential role of Ufm1 conjugation in the hematopoietic system. *Exp. Hematol.* **44**, 442–446 (2016).
22. K. Tatsumi, H. Yamamoto-Mukai, R. Shimizu, S. Waguri, Y. S. Sou, A. Sakamoto, C. Taya, H. Shitara, T. Hara, C. H. Chung, K. Tanaka, M. Yamamoto, M. Komatsu, The Ufm1-activating enzyme Uba5 is indispensable for erythroid differentiation in mice. *Nat. Commun.* **2**, 181 (2011).
23. M. Zhang, X. Zhu, Y. Zhang, Y. Cai, J. Chen, S. Sivaprakasam, A. Gurav, W. Pi, L. Makala, J. Wu, B. Pace, D. Tuan-Lo, V. Ganapathy, N. Singh, H. Li, RCAD/Ufl1, a Ufm1 E3 ligase, is essential for hematopoietic stem cell function and murine hematopoiesis. *Cell Death Differ.* **22**, 1922–1934 (2015).
24. A. Cañellas-Socias, C. Cortina, X. Hernando-Momblona, S. Palomo-Ponce, E. J. Mulholland, G. Turon, L. Mateo, S. Conti, O. Roman, M. Sevillano, F. Slebe, D. Stork, A. Caballé-Mestres, A. Berenguer-Llergo, A. Álvarez-Varela, N. Fenderico, L. Novellasdemunt, L. Jiménez-Gracia, T. Sipka, L. Bardia, P. Lorden, J. Colombelli, H. Heyn, X. Trepat, S. Tejpar, E. Sancho, D. V. F. Tauriello, S. Leedham, C. S.-O. Attolini, E. Batlle, Metastatic recurrence in colorectal cancer arises from residual $EMP1^{+}$ cells. *Nature* **611**, 603–613 (2022).
25. L. Masclef, O. Ahmed, B. Estavoyer, B. Larrivee, N. Labrecque, A. Nijnik, E. B. Affar, Roles and mechanisms of BAP1 deubiquitinase in tumor suppression. *Cell Death Differ.* **28**, 606–625 (2021).
26. R. Deng, Y. Guo, L. Li, J. He, Z. Qiang, H. Zhang, R. Chen, Y. Wang, X. Zhao, J. Yu, BAP1 suppresses prostate cancer progression by deubiquitinating and stabilizing PTEN. *Mol. Oncol.* **15**, 279–298 (2021).
27. B. H. Louie, R. Kurzrock, BAP1: Not just a BRCA1-associated protein. *Cancer Treat. Rev.* **90**, 102091 (2020).
28. Y. K. Xia, Y. R. Zeng, M. L. Zhang, P. Liu, F. Liu, H. Zhang, C. X. He, Y. P. Sun, J. Y. Zhang, C. Zhang, L. Song, C. Ding, Y. J. Tang, Z. Yang, C. Yang, P. Wang, K. L. Guan, Y. Xiong, D. Ye, Tumor-derived neomorphic mutations in ASXL1 impairs the BAP1-ASXL1-FOXK1/K2 transcription network. *Protein Cell* **12**, 557–577 (2021).
29. A. Dey, D. Seshasayee, R. Noubade, D. M. French, J. Liu, M. S. Chaurushiya, D. S. Kirkpatrick, V. C. Pham, J. R. Lill, C. E. Bakalarski, J. Wu, L. Phu, P. Katavolos, L. M. LaFave, O. Abdel-Wahab, Z. Modrusan, S. Seshagiri, K. Dong, Z. Lin, M. Balazs, R. Suriben, K. Newton, S. Hymowitz, G. Garcia-Manero, F. Martin, R. L. Levine, V. M. Dixit, Loss of the tumor suppressor BAP1 causes myeloid transformation. *Science* **337**, 1541–1546 (2012).
30. L. Gossage, T. Eisen, E. R. Maher, VHL, the story of a tumour suppressor gene. *Nat. Rev. Cancer* **15**, 55–64 (2015).
31. J. Guo, A. A. Chakraborty, P. Liu, W. Gan, X. Zheng, H. Inuzuka, B. Wang, J. Zhang, L. Zhang, M. Yuan, J. Novak, J. Q. Cheng, A. Toker, S. Signoretti, Q. Zhang, J. M. Asara, W. G. Kaelin Jr., W. Wei, pVHL suppresses kinase activity of Akt in a proline-hydroxylation-dependent manner. *Science* **353**, 929–932 (2016).
32. K. F. Chen, Y. Y. Lai, H. S. Sun, S. J. Tsai, Transcriptional repression of human *cad* gene by hypoxia inducible factor-1α. *Nucleic Acids Res.* **33**, 5190–5198 (2005).
33. B. Krishnamachary, D. Zagzag, H. Nagasawa, K. Rainey, H. Okuyama, J. H. Baek, G. L. Semenza, Hypoxia-inducible factor-1-dependent repression of *E-cadherin* in von Hippel-Lindau tumor suppressor-null renal cell carcinoma mediated by TCF3, ZFHX1A, and ZFHX1B. *Cancer Res.* **66**, 2725–2731 (2006).
34. S. Zhu, S. Deng, C. He, M. Liu, H. Chen, Z. Zeng, J. Zhong, Z. Ye, S. Deng, H. Wu, C. Wang, G. Zhao, Reciprocal loop of hypoxia-inducible factor-1α (HIF-1α) and metastasis-associated protein 2 (MTA2) contributes to the progression of pancreatic carcinoma by suppressing *E-cadherin* transcription. *J. Pathol.* **245**, 349–360 (2018).
35. J. J. Kim, S. B. Lee, J. Jang, S. Y. Yi, S. H. Kim, S. A. Han, J. M. Lee, S. Y. Tong, N. D. Vincelette, B. Gao, P. Yin, D. Evans, D. W. Choi, B. Qin, T. Liu, H. Zhang, M. Deng, J. Jen, J. Zhang, L. Wang, Z. Lou, WSB1 promotes tumor metastasis by inducing pVHL degradation. *Genes Dev.* **29**, 2244–2257 (2015).
36. X. Liu, X. Zhang, Z. Peng, C. Li, Z. Wang, C. Wang, Z. Deng, B. Wu, Y. Cui, Z. Wang, C. P. Cui, M. Zheng, L. Zhang, Deubiquitylase OTUD6B governs pVHL stability in an enzyme-independent manner and suppresses hepatocellular carcinoma metastasis. *Adv. Sci.* **7**, 1902040 (2020).
37. J. Liu, D. Guan, M. Dong, J. Yang, H. Wei, Q. Liang, L. Song, L. Xu, J. Bai, C. Liu, J. Mao, Q. Zhang, J. Zhou, X. Wu, M. Wang, Y. S. Cong, UFMylation maintains tumour suppressor p53 stability by antagonizing its ubiquitination. *Nat. Cell Biol.* **22**, 1056–1063 (2020).
38. M. Kang, S. G. Park, S. A. Lee, S. Kim, D. Lee, M. E. Shirbhate, S. Y. Youn, K. M. Kim, S. S. Cha, J. Kwon, Targeting BAP1 with small compound inhibitor for colon cancer treatment. *Sci. Rep.* **13**, 2264 (2023).
39. J. Tang, S. Xi, G. Wang, B. Wang, S. Yan, Y. Wu, Y. Sang, W. Wu, R. Zhang, T. Kang, Prognostic significance of BRCA1-associated protein 1 in colorectal cancer. *Med. Oncol.* **30**, 541 (2013).
40. M. Huang, T. Gao, X. Chen, J. Yi, X. Zhou, Circ_0087851 suppresses colorectal cancer malignant progression through triggering miR-593-3p/BAP1-mediated ferroptosis. *J. Cancer Res. Clin. Oncol.* **150**, 204 (2024).
41. W. G. Kaelin Jr., Von Hippel-Lindau disease: Insights into oxygen sensing, protein degradation, and cancer. *J. Clin. Invest.* **132**, e162480 (2022).

42. Y. Li, X. Zhang, Y. Gao, J. Shi, L. Tang, G. Sui, G-quadruplexes in the BAP1 promoter positively regulate its expression. *Exp. Cell Res.* **369**, 147–157 (2018).
43. X. Zhang, Y. Zhou, Z. Shi, Z. Liu, H. Chen, X. Wang, Y. Cheng, L. Xi, X. Li, C. Zhang, L. Bao, C. Xuan, Integrated analysis of genes encoding ATP-dependent chromatin remodellers identifies CHD7 as a potential target for colorectal cancer therapy. *Clin. Transl. Med.* **12**, e953 (2022).
44. Z. Xiong, P. Xia, X. Zhu, J. Geng, S. Wang, B. Ye, X. Qin, Y. Qu, L. He, D. Fan, Y. Du, Y. Tian, Z. Fan, Glutamylation of deubiquitinase BAP1 controls self-renewal of hematopoietic stem cells and hematopoiesis. *J. Exp. Med.* **217**, e20190974 (2020).
45. Y. Cai, W. Pi, S. Sivaprakasam, X. Zhu, M. Zhang, J. Chen, L. Makala, C. Lu, J. Wu, Y. Teng, B. Pace, D. Tuan, N. Singh, H. Li, UFBP1, a key component of the Ufm1 conjugation system, is essential for ufmylation-mediated regulation of erythroid development. *PLOS Genet.* **11**, e1005643 (2015).
46. B. Qin, J. Yu, S. Nowsheen, M. Wang, X. Tu, T. Liu, H. Li, L. Wang, Z. Lou, UFL1 promotes histone H4 ufmylation and ATM activation. *Nat. Commun.* **10**, 1242 (2019).
47. Z. Wang, Y. Gong, B. Peng, R. Shi, D. Fan, H. Zhao, M. Zhu, H. Zhang, Z. Lou, J. Zhou, W. G. Zhu, Y. S. Cong, X. Xu, MRE11 UFMylation promotes ATM activation. *Nucleic Acids Res.* **47**, 4124–4135 (2019).
48. Y. Wen, H. Wang, X. Yang, Y. Zhu, M. Li, X. Ma, L. Huang, R. Wan, C. Zhang, S. Li, H. Jia, Q. Guo, X. Lu, Z. Li, X. Shen, Q. Zhang, L. Si, C. Yin, T. Liu, Pharmacological targeting of casein kinase 1δ suppresses oncogenic NRAS-driven melanoma. *Nat. Commun.* **15**, 10088 (2024).
49. T. Liu, J. Yu, M. Deng, Y. Yin, H. Zhang, K. Luo, B. Qin, Y. Li, C. Wu, T. Ren, Y. Han, P. Yin, J. Kim, S. Lee, J. Lin, L. Zhang, J. Zhang, S. Nowsheen, L. Wang, J. Boughey, M. P. Goetz, J. Yuan, Z. Lou, CDK4/6-dependent activation of DUB3 regulates cancer metastasis through SNAIL1. *Nat. Commun.* **8**, 13923 (2017).
50. Y. Wen, X. Yang, S. Li, L. Huang, J. Chen, L. Tan, X. Ma, Y. Zhu, Z. Li, C. Shan, C. Zhang, Q. Zhang, M. Liang, H. Zhang, T. Liu, Targeting CDK4/6 suppresses colorectal cancer by destabilizing YAP1. *MedComm* **6**, e70103 (2025).
51. Q. Long, K. Rabi, Y. Cai, L. Li, S. Huang, B. Qian, Y. Zhong, Z. Qi, Y. Zhang, K. Huang, X. Wang, L. Chang, W. Xie, H. Jiang, H. Zhang, J. Zhang, T. Ren, Z. Wang, T. Teesalu, C. Wu, L. Lu, Z. Zhu, Y. Chu, H. A. Santos, Z. Liu, Q. Zhao, X. Ye, Identification of splenic IRF7 as a nanotherapy target for tele-conditioning myocardial reperfusion injury. *Nat. Commun.* **16**, 1909 (2025).
52. B. Győrffy, Integrated analysis of public datasets for the discovery and validation of survival-associated genes in solid tumors. *Innovation* **5**, 100625 (2024).
53. M. Sun, L. Li, Y. Niu, Y. Wang, Q. Yan, F. Xie, Y. Qiao, J. Song, H. Sun, Z. Li, S. Lai, H. Chang, H. Zhang, J. Wang, C. Yang, H. Zhao, J. Tan, Y. Li, S. Liu, B. Lu, M. Liu, G. Kong, Y. Zhao, C. Zhang, S.-H. Lin, C. Luo, S. Zhang, C. Shan, PRMT6 promotes tumorigenicity and cisplatin response of lung cancer through triggering 6PGD/ENO1 mediated cell metabolism. *Acta Pharm. Sin. B* **13**, 157–173 (2023).

Acknowledgments

Funding: This work was supported by National Natural Science Foundation of China (82473109, 82404654, and U21A20379), the Science and Technology Project of Guangdong Province (2023A0505050149), the Pearl River Talents Scheme of Guangdong Province (2019QN01Y933 and 2019QN01Y990), Guangdong Major Project of Basic and Applied Basic Research (2023B0303000026), Guangdong Basic and Applied Basic Research Foundation (2025A1515012357, 2024A1515013266 and 2024B1515040007), China Postdoctoral Science Foundation (2024 M750581), the National Key Research and Development Program of China (2021YFA1101000 and 2021YFA1101004), Research Fund for Foreign Scholars of China (82250710176), leading innovation and entrepreneurship team of Hangzhou (TD2020006), and Medical Joint Fund of Jinan University (YXJC2022006). O.J.L. acknowledges the support of K. C. Wong Education Foundation. The funders had no role in study design, data collection and analysis, decision to publish, or preparation of the paper. **Author contributions:** Conceptualization: X.Y., L.H., H.G., and T.L. Methodology: X.Y., Y.W., L.H., M.L., R.W., J.C., H.G., X.S., and T.L. Software: Y.Z. Validation: X.Y., Y.W., C.Z., L.H., M.L., X.M., R.W., J.C., X.S., and T.L. Formal analysis: X.Y., Y.W., C.Z., J.C., O.J.L., and T.L. Investigation: X.Y., Y.W., S.Q., Y.Z., L.H., M.L., X.M., R.W., J.C., O.J.L., and X.S. Resources: X.Y., Y.W., S.Q., Y.Z., C.Z., L.H., R.W., J.C., H.G., and X.S. Data curation: Y.W. Writing—original draft: X.Y., Y.W., S.Q., C.Z., C.R.G., R.C., and T.L. Writing—review and editing: X.Y., Y.W., L.H., H.G., C.R.G., O.J.L., X.S., R.C., and T.L. Visualization: X.Y., Y.W., Y.Z., C.Z., O.J.L., X.S., and T.L. Supervision: X.Y., R.H., X.S., R.C., and T.L. Project administration: X.Y., C.Z., R.C., and T.L. Funding acquisition: Y.W., S.Q., X.S., R.C., and T.L. **Competing interests:** The authors declare that they have no competing interests. **Data and materials availability:** All data needed to evaluate the conclusions in the paper are present in the paper and/or the Supplementary Materials.

Submitted 16 October 2024
Accepted 10 June 2025
Published 11 July 2025
10.1126/sciadv.adt8800